4th December

Jeong, S. J., Schimel, D., Frankenberg, C., Drewry, D. T., Fisher, J. B., Verma, M., ... & Joiner, J. (2017). Application of satellite solar-induced chlorophyll fluorescence to understanding large-scale variations in vegetation phenology and function over northern high latitude forests. *Remote sensing of environment*, *190*, 178-187.

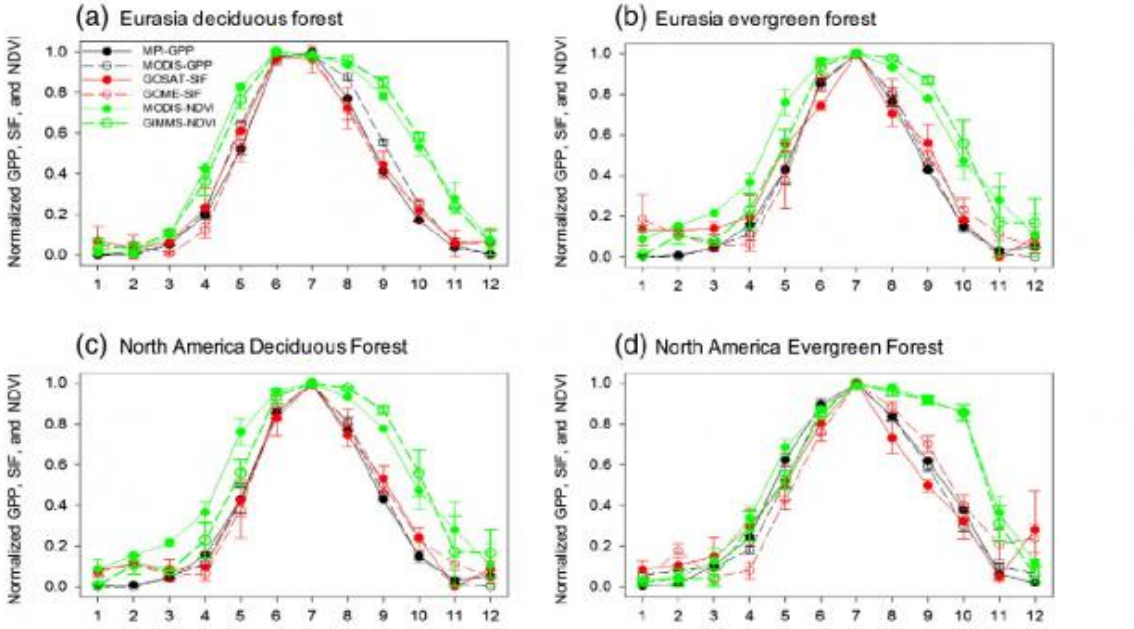

Fig. 2. Normalized mean seasonal cycle of area averaged GOSAT SIF, GOME SIF, MODIS NDVI, GIMMS NDVI, MPI GPP, and MODIS GPP over northern temperate and boreal forests (40–55°N) for the period 2010–2012 in deciduous and evergreen forests over Eurasia (a, b) and over North America (c, d). Error bars in all figures indicate monthly standard deviations for the period 2010–2012.

The author observed that both NDVI and SIF linearly increased with temperature increases throughout the spring. However, in the fall, although NDVI linearly responded to temperature increases, SIF and GPP did not linearly increase with temperature increases, implying a seasonal hysteresis of SIF and GPP in response to temperature
changes across boreal ecosystems throughout their growing season. Seasonal hysteresis of vegetation at large-scales is consistent with the known phenomena that light limits boreal forest ecosystem productivity in the fall.

3rd December

Migliavacca, M., Perez-Priego, O., Rossini, M., El-Madany, T. S., Moreno, G., van der Tol, C., ... & Carrara, A. (2017). Plant functional traits and canopy structure control the relationship between photosynthetic CO 2 uptake and far-red sun-induced fluorescence in a Mediterranean grassland under different nutrient availability. *New Phytologist*, *214*(3), 1078-1091.

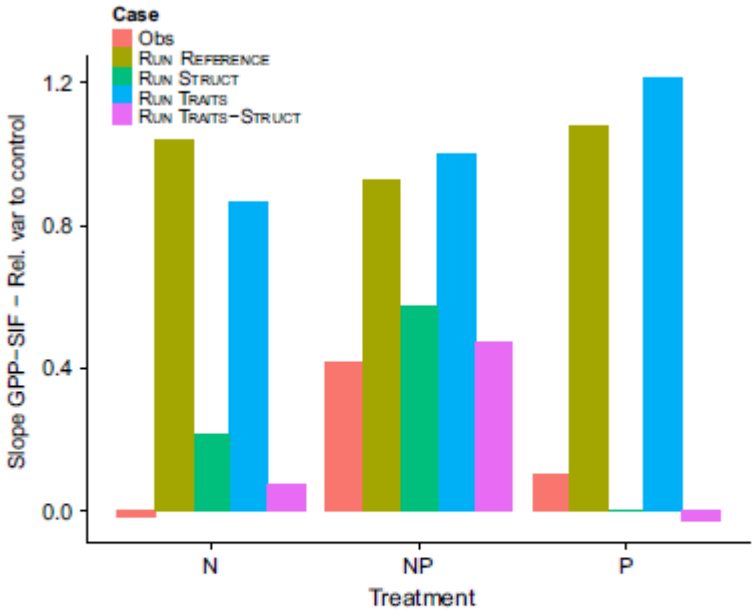

Fig. 7 Histogram reporting the change of the fluorescence emission at 760 nm vs gross primary productivity (F_{760}–GPP) slope under the nitrogen (N), phosphorus (P) and nitrogen–phosphorous (NP) addition treatments relative to the slope observed in the carbon (C) treatment. Different bars indicate different treatments.

The author analyzed the structural and functional factors controlling the emission of SIF at 760 nm (F760) in a Mediterranean grassland manipulated with nutrient addition of nitrogen (N), phosphorous (P) or nitrogen–phosphorous (NP). Using the soil–canopy observation of photosynthesis and energy (SCOPE) model, we investigated how nutrient-induced changes in canopy structure (i.e. changes in plant forms abundance that influence leaf inclination distribution function, LIDF) and functional traits (e.g. N content in dry mass of leaves, N%, Chlorophyll a+b concentration (Cab) and maximum carboxylation capacity (Vcmax)) affected the observed linear relationship between F760 and GPP. The author concluded that the addition of nutrients imposed a change in the abundance of different plant forms and biochemistry of the canopy that controls F760. Changes in canopy structure mainly control the GPP–F760 relationship, with a secondary effect of Cab and Vcmax.

In order to evaluate the effects of fertilized-induced changes in functional traits (Cab, Vcmax) and canopy structure (specifically LIDFa, LIDFb) on the simulated F760 signal and on the GPP– F760 relationship, we performed a factorial modeling experiment with four cases. In all cases, the parameters varied in time (i.e. between field campaigns) to account for phenology.

RUN REFERENCE:
LIDFa, LIDFb, Vcmax and Cab fixed across treatments to the mean estimates of the C treatment;

RUN TRAITS:
Vcmax and Cab variable across treatments to account for differences in functional traits induced by fertilization. LIDFa and LIDFb fixed across treatments, only variable in time;

RUN STRUCT:
LIDFa and LIDFb variable across treatments to account for differences in canopy structure induced by changes in composition of plant
forms after the fertilization. Vcmax and Cab fixed across treatments, only variable in time;

RUN TRAITS–STRUCT:
both structural parameters (LIDFa, LIDFb) and traits (Vcmax and Cab) variable across treatments.

2nd December

Cui, T., Sun, R., Qiao, C., Zhang, Q., Yu, T., Liu, G., & Liu, Z. (2017). Estimating Diurnal Courses of Gross Primary Production for Maize: A Comparison of Sun-Induced Chlorophyll Fluorescence, Light-Use Efficiency and Process-Based Models. *Remote Sensing*, *9*(12), 1267.

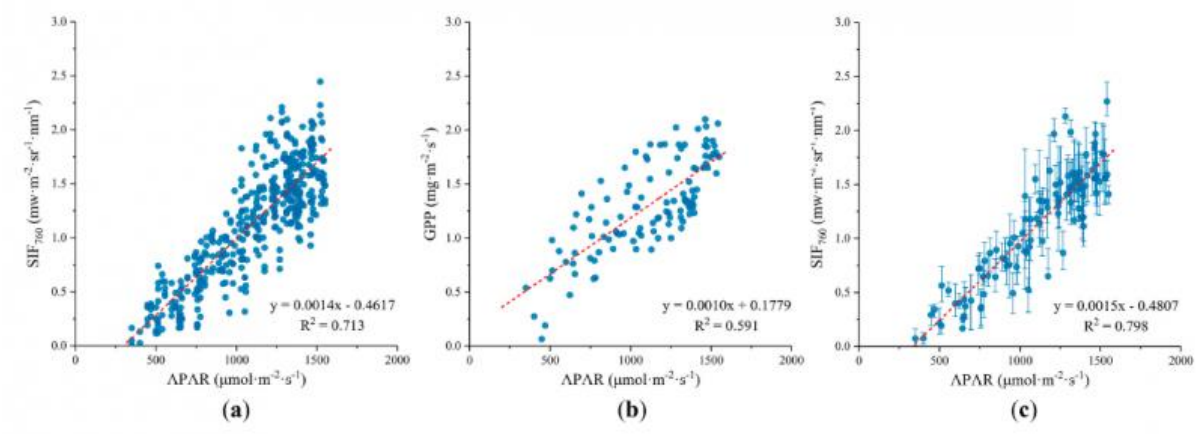

Figure 4. Relationship between APAR (absorbed photosynthetically active radiation) and: (**a**) individual SIF_{760}; (**b**) GPP; and (**c**) averaged SIF. The error bar indicates the range of SIF_{760} values for four measurements.

Our results showed that both SIF760 and GPP were linearly correlated with APAR, and the SIF760-GPP relationship was adequately characterized using a linear function. The evaluation of the modeled GPP against the GPP measured from the tower demonstrated that all three approaches provided reasonable estimates. However, I think the relationship between APAR and GPP seems quite hysteresis.

1st December

Wei, Xiaoxu., Wang, Xufen., Wei, Wei., Wan, Wei. (2018). Use of Sun-Induced Chlorophyll Fluorescence Obtained by OCO-2 and GOME-2 for GPP Estimates of the Heihe River Basin, China, Remote Sensing.

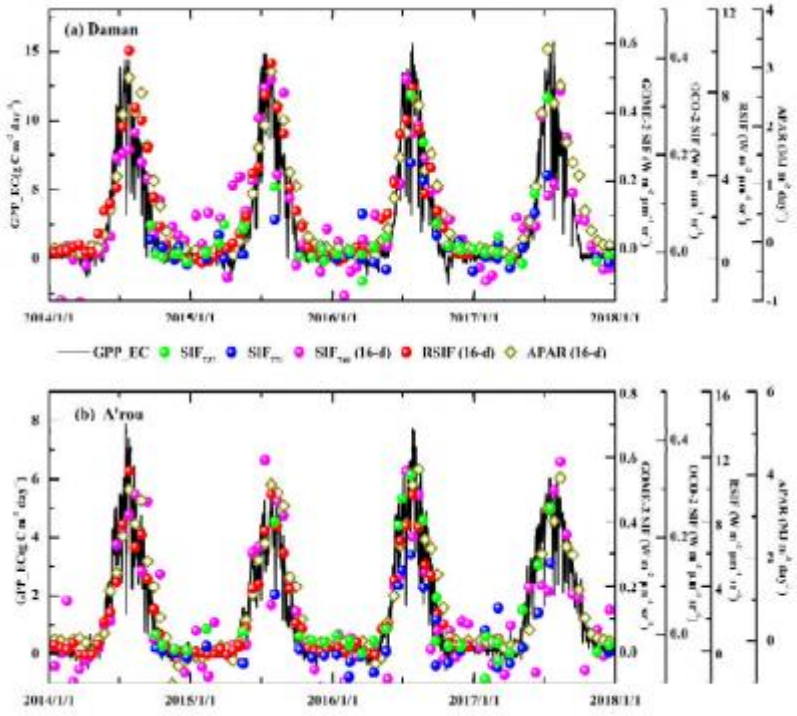

Figure 2. Seasonal cycles of SIF757, SIF771, SIF740 (16-d), RSIF (16-d), APAR (16-d), and tower GPP for the period 2014–2017 at the (a) Daman and (b) A'rou sites.

This paper found that the robustness of the correlation coefficients of OCO-2 SIF with GOME-2 SIF was highly dependent on the size of their spatial footprint overlaps, indicating that the spatial differences between OCO-2 and GOME-2 footprints contribute to the differences in GPP estimates between OCO-2 and GOME-2. In addition, the differences of viewing zenith angle (VZA), cloud contamination, scale effects, and environmental scalars (Tscalar × Wscalar) can result in differences between OCO-2 SIF and GOME-2 SIF. I think it would be better if there were field observations in these articles.

4th November

Pan, Y., Birdsey, R. A., Fang, J., Houghton, R., Kauppi, P. E., Kurz, W. A., ... & Ciais, P. (2011). A large and persistent carbon sink in the world's forests. *Science*, 1201609.

I think this paper well collected the data and anlysis. They used ground inventory data. The fluxes comprise a net global forest sink of 1.1 T 0.8 Pg C year−1, with tropical estimates having the largest uncertainties. Total forest sink estimate is equivalent in magnitude to the terrestrial sink deduced from fossil fuel emissions and land-use change sources minus ocean and atmospheric sinks! However, I think our ground inventory data is really minimum to estimate global carbon flux (Schimel et al., 2015).

3rd November

Walther, G. R., Post, E., Convey, P., Menzel, A., Parmesan, C., Beebee, T. J., ... & Bairlein, F. (2002). Ecological responses to recent climate change. *Nature*, *416*(6879), 389.

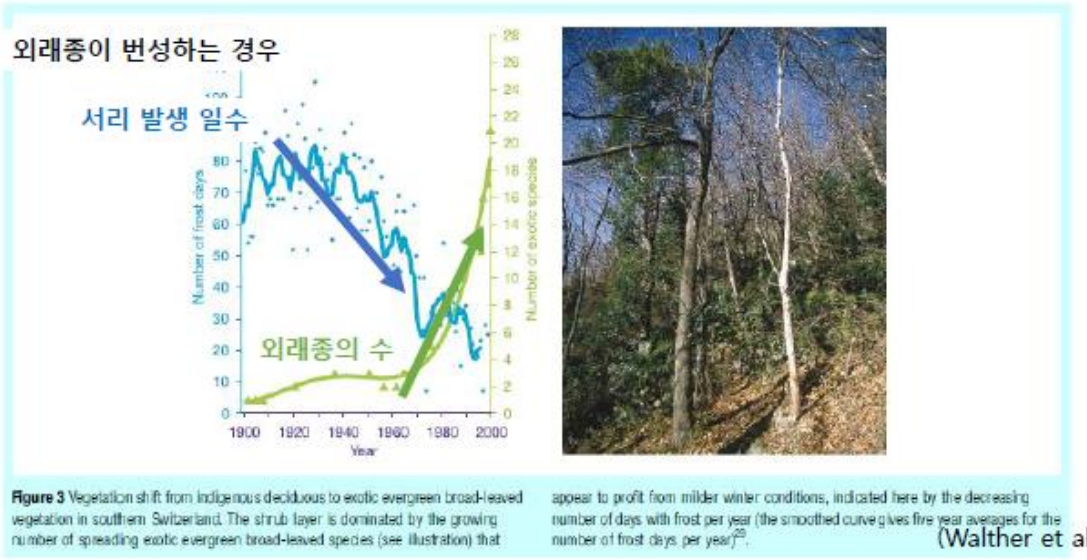

Figure 3 Vegetation shift from indigenous deciduous to exotic evergreen broad-leaved vegetation in southern Switzerland. The shrub layer is dominated by the growing number of spreading exotic evergreen broad-leaved species (see illustration) that appear to profit from milder winter conditions, indicated here by the decreasing number of days with frost per year (the smoothed curve gives five year averages for the number of frost days per year)[28].

(Walther et al., 2002)

I think this paper really well organized about "Ecological responses to recent climate change". I think one of the best review paper. Easy to read and well-organized table! If someone will start to study climate change, I will recommend this paper.

2nd November

Richardson, A. D. (2018). Tracking seasonal rhythms of plants in diverse ecosystems with digital camera imagery. *New Phytologist*.

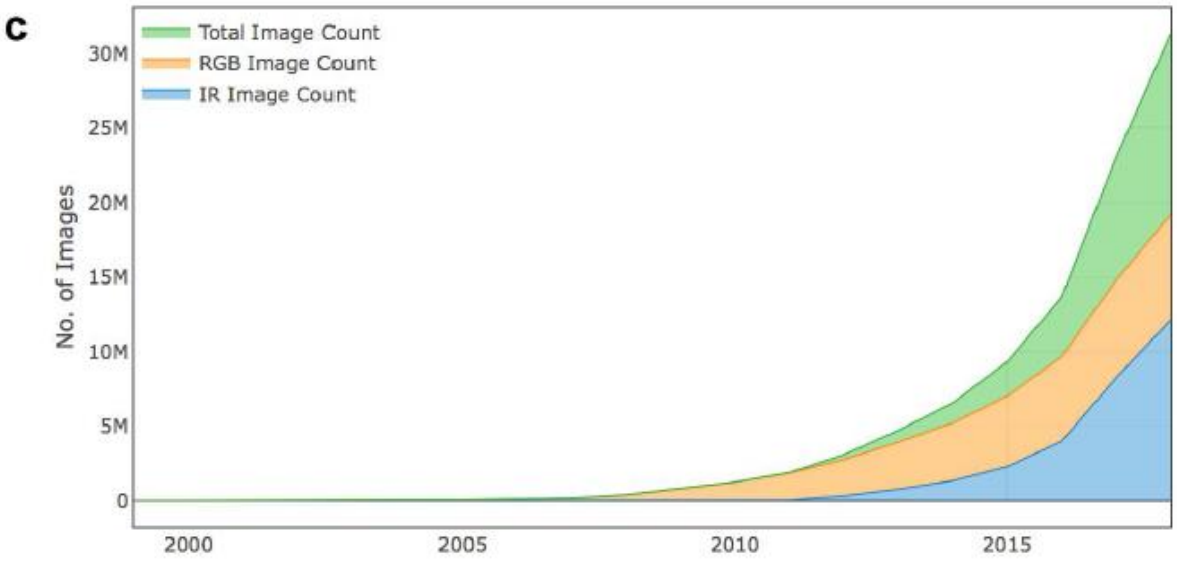

I think this paper is really well organized about "Phenocam". I think this kind of new method is really easy to estimate vegetation phenology and their physiology. The phenocam site is increasing. I hope the 4S will be a useful tool like this one.

1st November

Schimel, D. et al., 2015. Observing terrestrial ecosystems and the carbon cycle from space. *Global Change Biology*, *21*(5), 1762-1776.

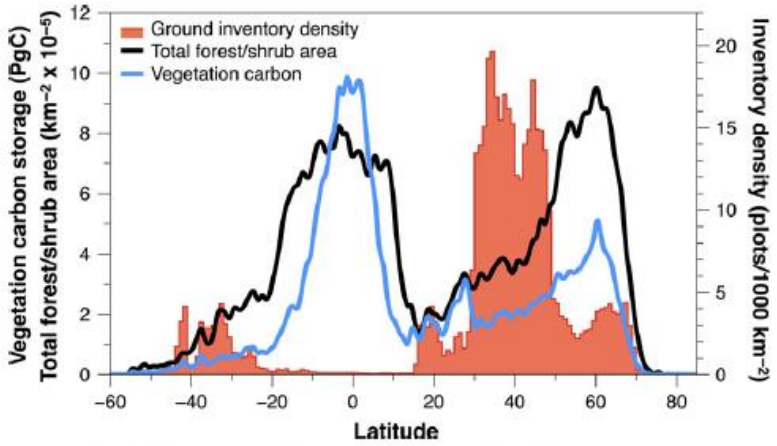

Fig. 5 The distribution of woody (forest and shrub land) area and biomass, estimated by radar–LiDAR fusion compared to data availability from forest inventory. The red histogram shows forest inventory plot density in plots 1000 km^{-2}. Similar to flux observations, biomass data is sparse in regions of maximum storage.

I chose this review paper to discuss the need to use satellite data and field observation together. This paper pointed out the field observation data does not represent global scales well, particularly in tropical and arctic regions. To overcome the weakness of field observation, a strategic combination of remote satellite and in situ data is required. However, there are still many limitations in field observation. I thought that near-surface sensors were expensive and slow to develop due to the monopoly of a company. To collect more in-situ data in critical regions, we concluded 1) collaboration with local people is necessary and 2) we should hit on a new way such as automatic drone to monitor vegetation.

4th October

Jacovides, C. P., Boland, J., Asimakopoulos, D. N., & Kaltsounides, N. A. (2010). Comparing diffuse radiation models with one predictor for partitioning incident PAR radiation into its diffuse component in the eastern Mediterranean basin. *Renewable Energy*, *35*(8), 1820-1827.

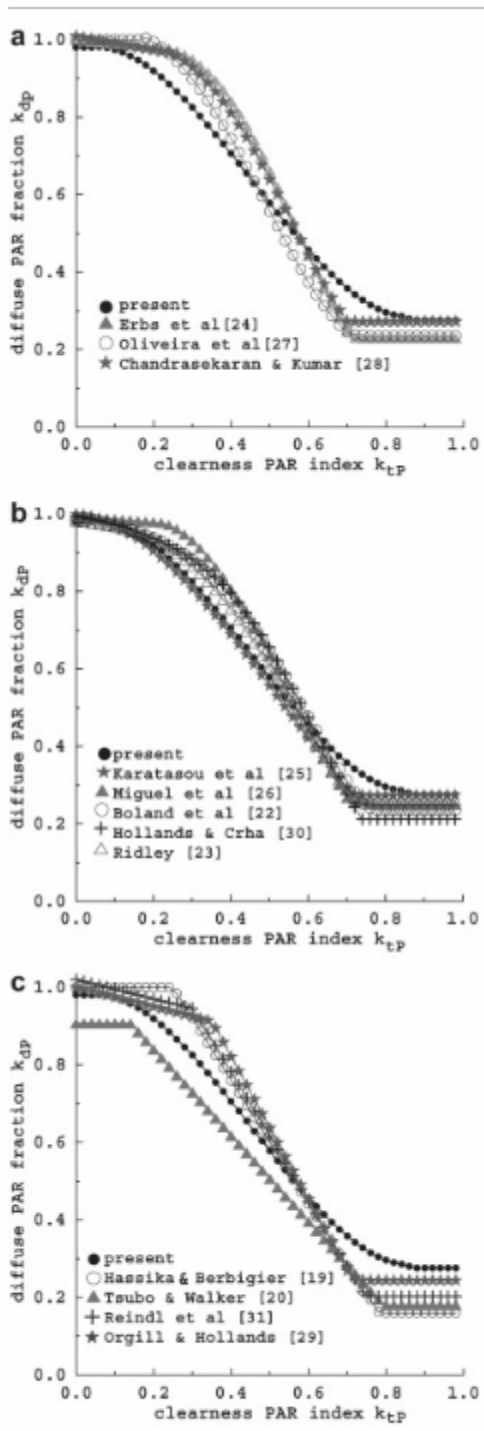

Download full-size image

Fig. 2. (a–c): The hourly diffuse PAR fraction (k_{dP}) versus hourly clearness PAR index (k_{tP}), showing standard and proposed correlations: (a) fourth-order polynomial correlations; (b) third-order and functional form correlations; and (c) first-order fittings.

This paper is about "**most of the candidate empirical models examined here appear to be location-independent for the diffuse PAR predictions**".

This study aiming to explore the applicability of several diffuse radiation empirical models, hourly measurements of diffuse PAR and global PAR irradiation collected at Athens from 1 January 2000 to 31 December 2002, are employed. These data were used to establish an empirical model relating the spectral diffuse fraction, kdP (ratio of the diffuse-to-global PAR) with the fractional transmission of global PAR ktP (ratio of the global PAR-to-extraterrestrial solar PAR).
The performance of the proposed empirical model was further compared with those of twelve other diffuse–global correlation models available in the literature in terms of the widely used statistical indicators mbe, rmse and t-test. From the overall analysis, it can be concluded that the proposed model predicts diffuse PAR values accurately, whereas most of the candidate empirical models examined here appear to be location-independent for the diffuse PAR predictions.

3rd October

Ma, S. et al., 2019. Application of the water-related spectral reflectance indices: A review. Ecological Indicators, 98: 68-79.

Table 5. Water-related indices having the same or similar band combinations, but different names.

Name	Abbreviation	Equation	Sensor and band wavelength	Application type	Reference
Modified NDWI	mNDWI	(GREEN − SWIR)/(GREEN + SWIR)	Landsat TM; GREEN = 0.52–0.60 and SWIR = 1.55–1.75	Surface water bodies detection	Xu (2006)
Normalized Difference Pond Index	NDPI (opposite to mNDWI)	(SWIR − GREEN)/(SWIR + GREEN)	SPOT-5; GREEN = 0.5–0.59 and SWIR = 1.58–1.75	Surface water bodies detection	Lacaux et al. (2007)
Infrared Index	II	(NIR − SWIR)/(NIR + SWIR)	A three band radiometer; NIR = 0.76–0.90 and SWIR = 1.55–1.75	Vegetation water detection	Hardisky et al. (1983)
SWIR based Vegetation Index	SWVI (same as II)	(NIR − SWIR)/(NIR + SWIR)	SPOT-VEGETATION, NIR = 0.78–0.89 and SWIR = 1.58–1.75	Vegetation water detection	Cayrol et al. (2000)
Normalized Difference Moisture Index	NDMI (same as II)	(NIR − MIR)/(NIR + MIR)	Landsat TM; NIR = 0.76–0.90 and MIR = 1.55–1.75	Vegetation water detection	Wilson and Sader (2002)
Land Surface Water Index	LSWI (same as II)	(NIR − SWIR)/(NIR + SWIR)	SPOT-VEGETATION, NIR = 0.78–0.89 and	Vegetation water detection	Xiao et al. (2004)

Wow! I think this paper is really well organized about water index. I should use many water index to estimate vegetation water detection in CCS project. What an interesting paper!

2nd October

Hu, J., Liu, L., Guo, J., Du, S., & Liu, X. (2018). Upscaling Solar-Induced Chlorophyll Fluorescence from an Instantaneous to Daily Scale Gives an Improved Estimation of the Gross Primary Productivity. *Remote Sensing*, *10*(10), 1663.

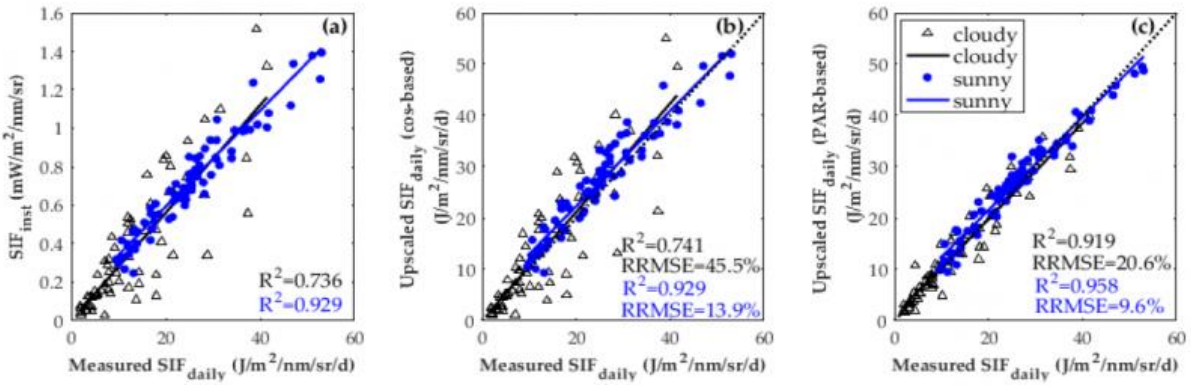

Figure 6. Scatter diagrams between the measured SIF_{daily} with SIF_{inst} (**a**) and the upscaled SIF_{daily} using the cos-based (**b**) and PAR-based (**c**) methods for sunny and cloudy days at two sites, as indicated by the colors. The black dotted line represents the 1:1 line.

In this study, the authors present a SIF upscaling method using photosynthetically active radiation (PAR) as a driving variable. In addition, they compared SIF upscaling method using cos(SZA). In this paper, they assume there is no such big diurnal variation in APAR and the SIF have the strong linear relationship with PAR in diurnal scale. My question is if the SIF is shown a linear relationship with PAR, then why do we need to estimate SIF diurnal pattern? I mean just to estimate GPP by using PAR will be better. What about NIRvP?

1st October

Cruse, M. J., Kucharik, C. J., & Norman, J. M. (2015). Using a simple apparatus to measure direct and diffuse photosynthetically active radiation at remote locations. *PloS one*, *10*(2), e0115633.

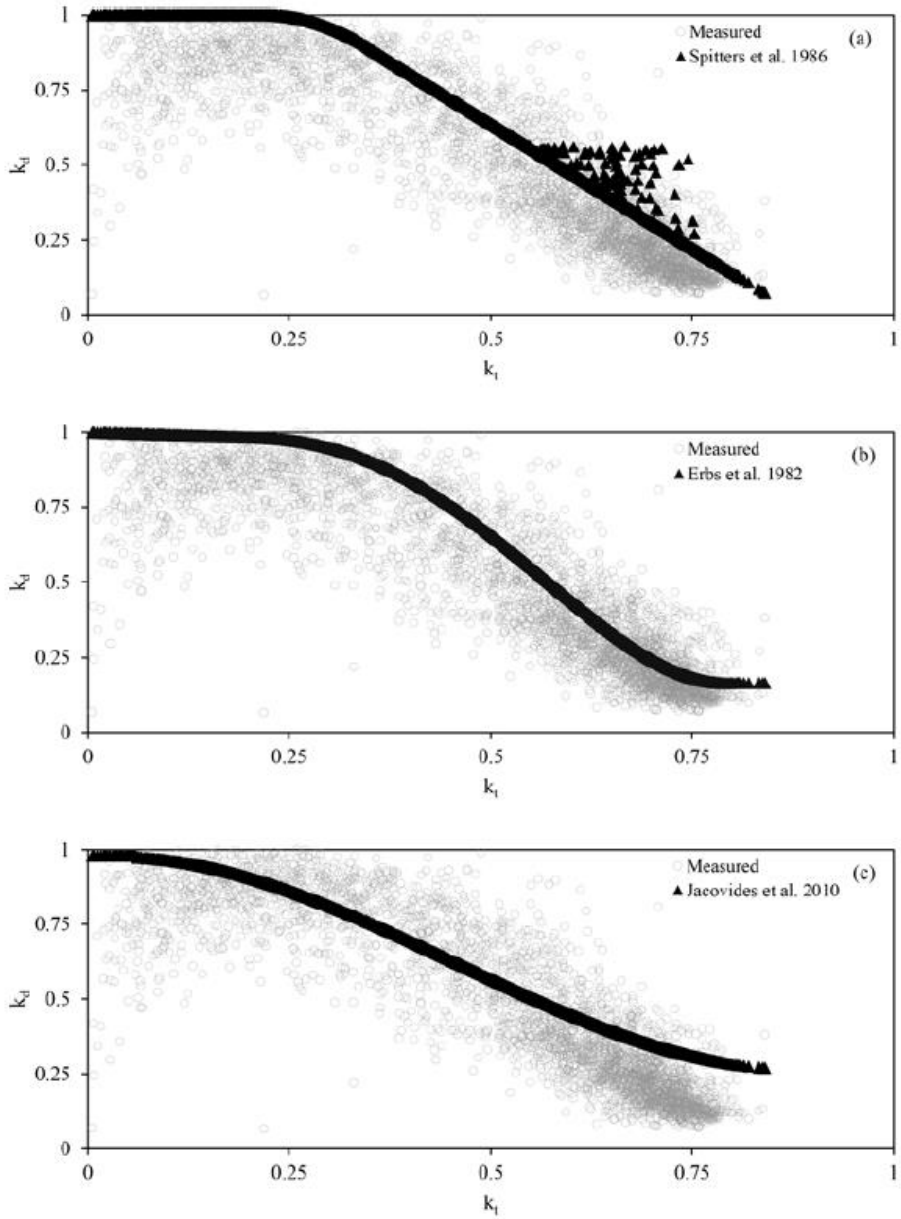

Figure 5. Relationship between clearness index (k_t) and ratio of diffuse-to-global radiation (k_d) for observed values plus 3 modeling approaches. a) Spitters et al. 1986 b) Erbs et al. 1982 c) Jacovides et al. 2010

I think this paper is really nice about rotating band system to measure diffuse PAR ratio. I did not know this paper before making our system. The author also used banded arm to block the direct beam. What an interested in. Also, in this paper, the author provided the calibration sheet for the reader. I think if I have time, or after developing our new method, I can try it.

4th September

Wohlfahrt, G., Gerdel, K., Migliavacca, M., Rotenberg, E., Tatarinov, F., Müller, J., ... & Yakir, D. (2018). Sun-induced fluorescence and gross primary productivity during a heat wave. *Scientific reports*, *8*(1), 14169.

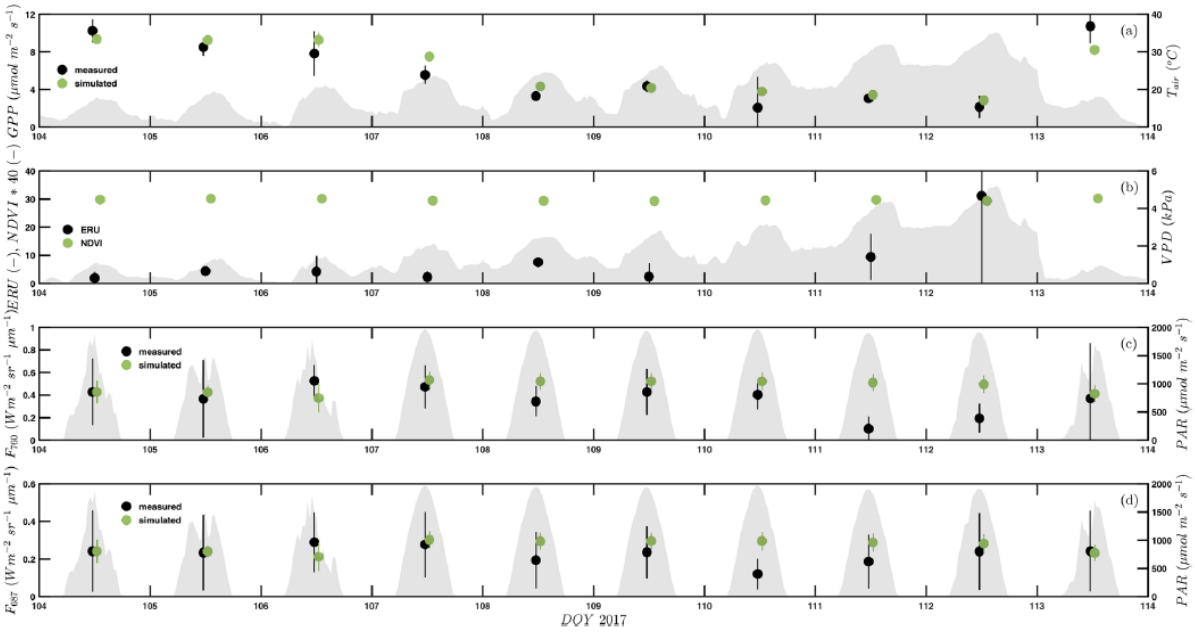

Figure 2. Midday (10–14 local time) mean (±standard deviation) (**a**) inferred gross primary productivity (GPP, μmol m^{-2} s^{-1}), (**b**) the ecosystem relative uptake rate (ERU) and the normalised difference vegetation index (NDVI from hyperspectral sensor), and sun-induced fluorescence in the (**c**) O_2-A (F_{760}) and (**d**) O_2-B (F_{687}) band (W m^{-2} sr^{-1} μm^{-1}) during the heat wave and the first day thereafter. Hourly air temperature (T_{air}, °C), vapour pressure deficit (VPD, kPa) and incident photosynthetically active radiation (PAR, μmol m^{-2} s^{-1}) are shown in panels a-d as grey shading. Simulated SIF is scaled to the measured value during the first day of the heat wave (see Methods). Simulated GPP and SIF (green symbols) are slightly offset horizontally from measured values (black symbols) for improved clarity.

I think this paper quite well showed the strength of SIF. I was interested in such points to follow as:

1) APAR, SIF, and NEE relationship

2) O2A and O2B response to the heat wave

GPP decreased linearly during the course of the heat

GPP decreased linearly during the course of the heat wave, while SIF declined slightly initially and then dropped dramatically during the peak of the heat wave, temporally coinciding with a biochemical impairment of photosynthesis inferred from the increase in the uptake ratio of carbonyl sulfide to carbon dioxide.

Measured F687, except for a 50% reduction on the seventh day of the heat wave (DOY 110), remained near constant during the entire heat wave (Fig. 2c), while F760 was near constant during the earlier part of the heat wave, followed by a pronounced decrease during the last two days (DOY 111.112; Fig. 2d).

3rd September

Song, X. P., Hansen, M. C., Stehman, S. V., Potapov, P. V., Tyukavina, A., Vermote, E. F., & Townshend, J. R. (2018). Global land change from 1982 to 2016. *Nature*, *560*(7720), 639.

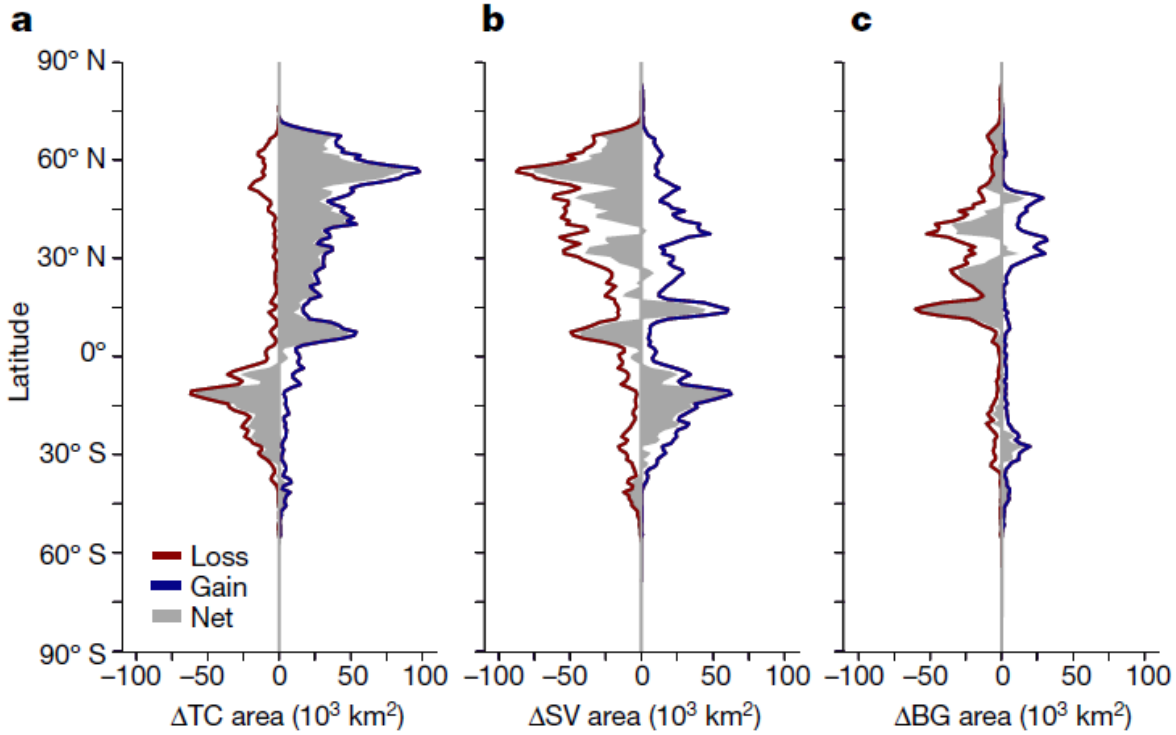

Fig. 2 | Latitudinal profiles of change in land cover from 1982 to 2016. **a**, Tree canopy cover change (ΔTC). **b**, Short vegetation cover change (ΔSV). **c**, Bare ground cover change (ΔBG). Area statistics were calculated for every 1° of latitude.

This paper showed that contrary to the prevailing view that forest area has declined globally - three cover has increased by 2.24 million km2. In addition, of all land changes, 60% are associated with direct human activities and 40% with indirect drivers such as climate change. The reason why I like this paper is this paper tried to monitor understory vegetation. If I have time, I will try to analysis understory phenology and compare to overstory.

2nd September

Marcolla, B., & Cescatti, A. (2017). The geometry of the hemispherical radiometric footprint over plant canopies. *Theoretical and Applied Climatology*, 1-10.

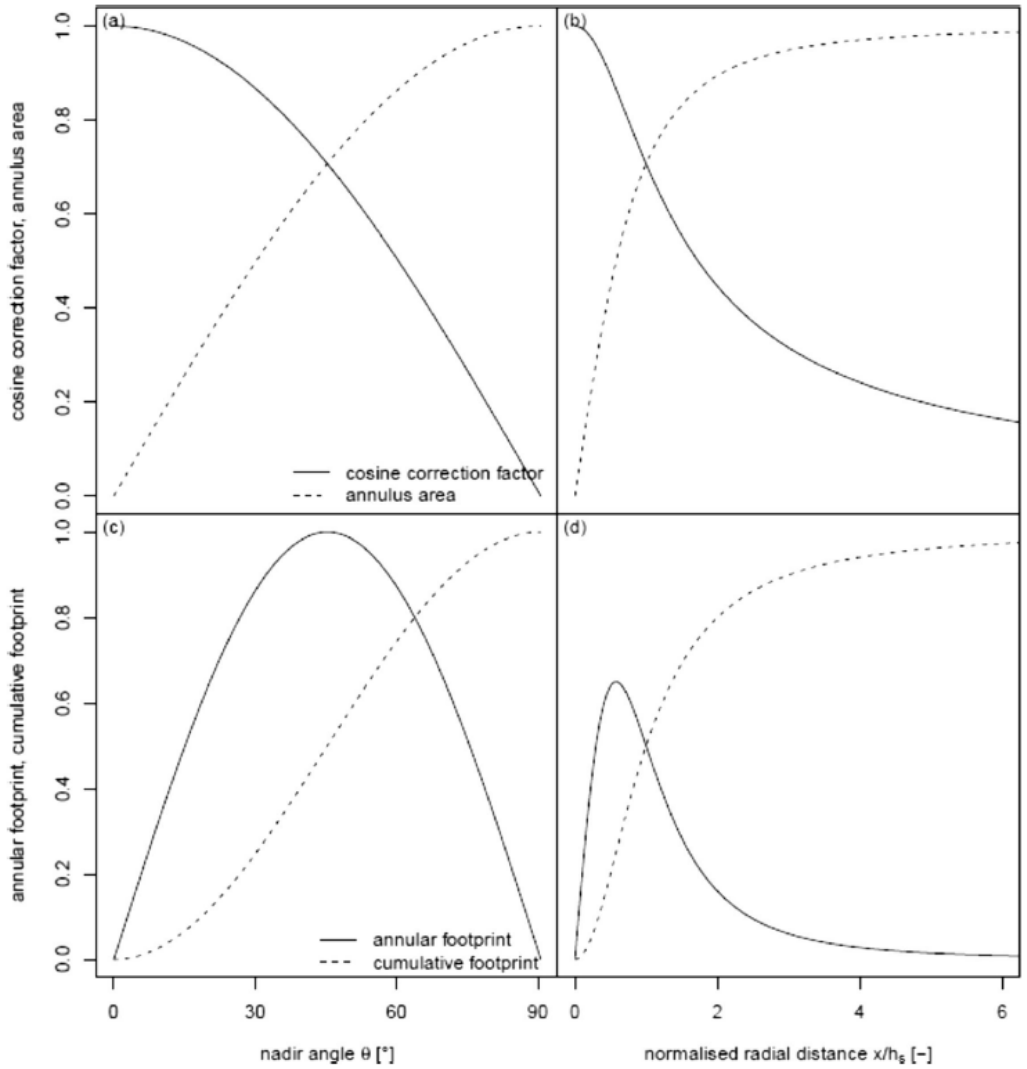

Fig. 2 Cosine correction factor and area of the annulus as a function of the nadir angle θ (a) and of the normalized radial distance x/h_s (b). Radiative annular footprint function (solid line) and cumulative footprint (dashed line) above a bare surface as a function of the (c) nadir angle and of the (d) radial distance

I think this paper is well-made paper because this paper helps us to solve measuring Geometry of the hemispherical radiometric footprint. This paper figures out that in order to achieve comparable extensions of the footprint areas, hemispherical radiometric measurements should, therefore, be taken about 6-15 times higher than turbulent flux ones, depending on the vegetation type. This means, when we compare spectral data to flux data, it should have always bias.

1st September

Liu, X., & Liu, L. (2018). Influence of the canopy BRDF characteristics and illumination conditions on the retrieval of solar-induced chlorophyll fluorescence. *International Journal of Remote Sensing*, *39*(6), 1782-1799.

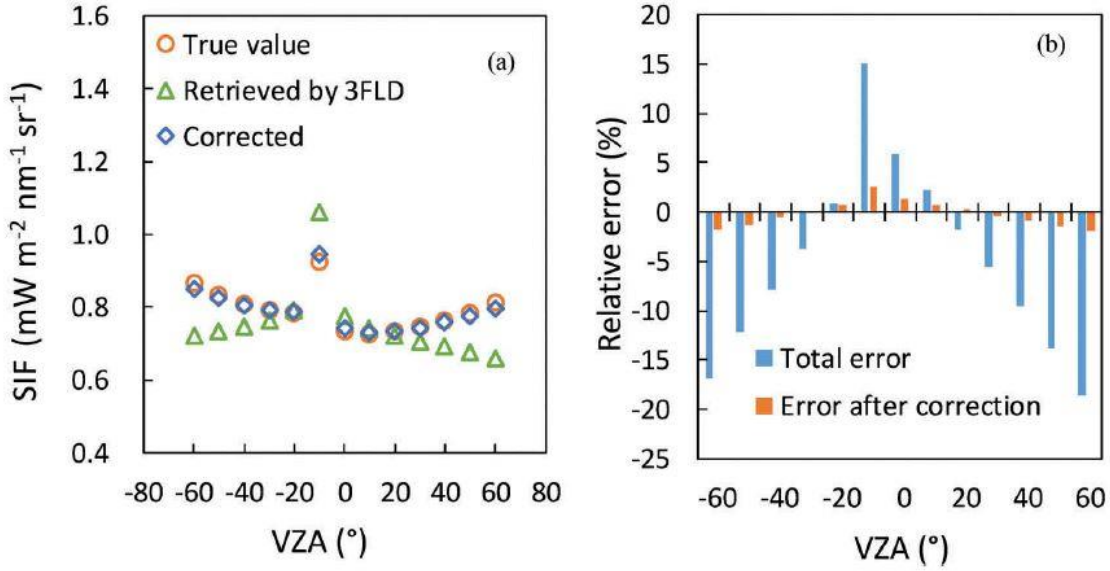

Figure 8. (a) The reference SIF values along with the retrieved values before and after the correction for the direct radiation in-filling effect at the O_2-A band in the solar principal plane and for a solar zenith angle of 10°. (b) The relative errors in the retrieved SIF with and without the correction for direct radiation in-filling.

This study thus provides a possible approach to estimating and correcting for the direct radiation-infilling effect using prior knowledge of the bidirectional reflectance distribution function characteristics of direct and diffuse radiation for specific targets. I could not understand full manuscript, but I will use MODTRAN software to correct atmospheric correction. I will keep reading this paper.

4th August

Fournier, A., Goulas, Y., Daumard, F., Ounis, A., Champagne, S., & Moya, I. (2014, April). Effects of vegetation directional reflectance on sun-induced fluorescence retrieval in the oxygen absorption bands. In *Proc. of 5th Int. Workshop on Remote Sensing of Vegetation Fluorescence* (pp. 1-5).

The illumination term was simulated using MODTRAN 4. The figure 3 present diurnal evolution of diffuse fraction and the depth of diffuse a direct radiation for the spectral bands and resolution of the Instrument used for acquisition on senescent wheat.

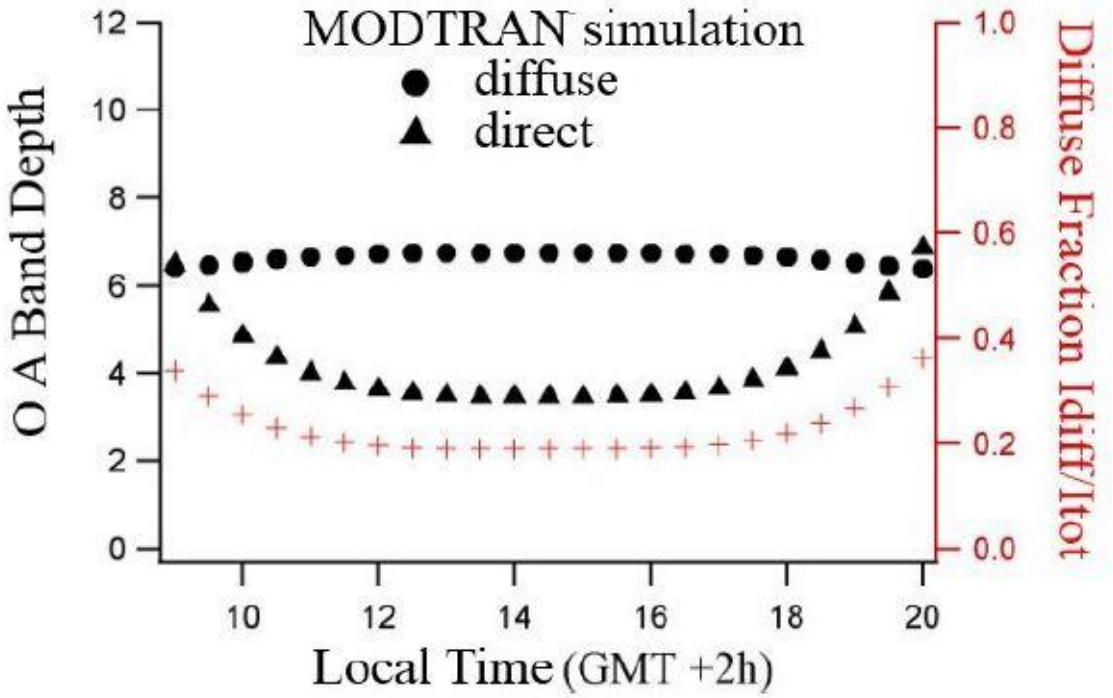

Figure 3: Diurnal evolution of direct and diffuse Irradiance depth and diffuse fraction simulated with MODTRAN4.

I think this paper also quite interesting because this paper showed experimental evidence of a bias by comparing reflected and incoming sunlight under different illumination regimes. In the abstract, I found the sentence about diffuse light experienced a longer optical path, and have a great absorption band depth than direct light. In addition, this paper showed the evidence by a using the MODTRAN model. It was interesting because I will use this theory to the next paper!

3rd August

Zuromski, L. M., Bowling, D. R., Köhler, P., Frankenberg, C., Goulden, M. L., Blanken, P. D., & Lin, J. C. (2018). Solar-Induced Fluorescence

Detects Interannual Variation in Gross Primary Production of Coniferous Forests in the Western United States. *Geophysical Research Letters*.

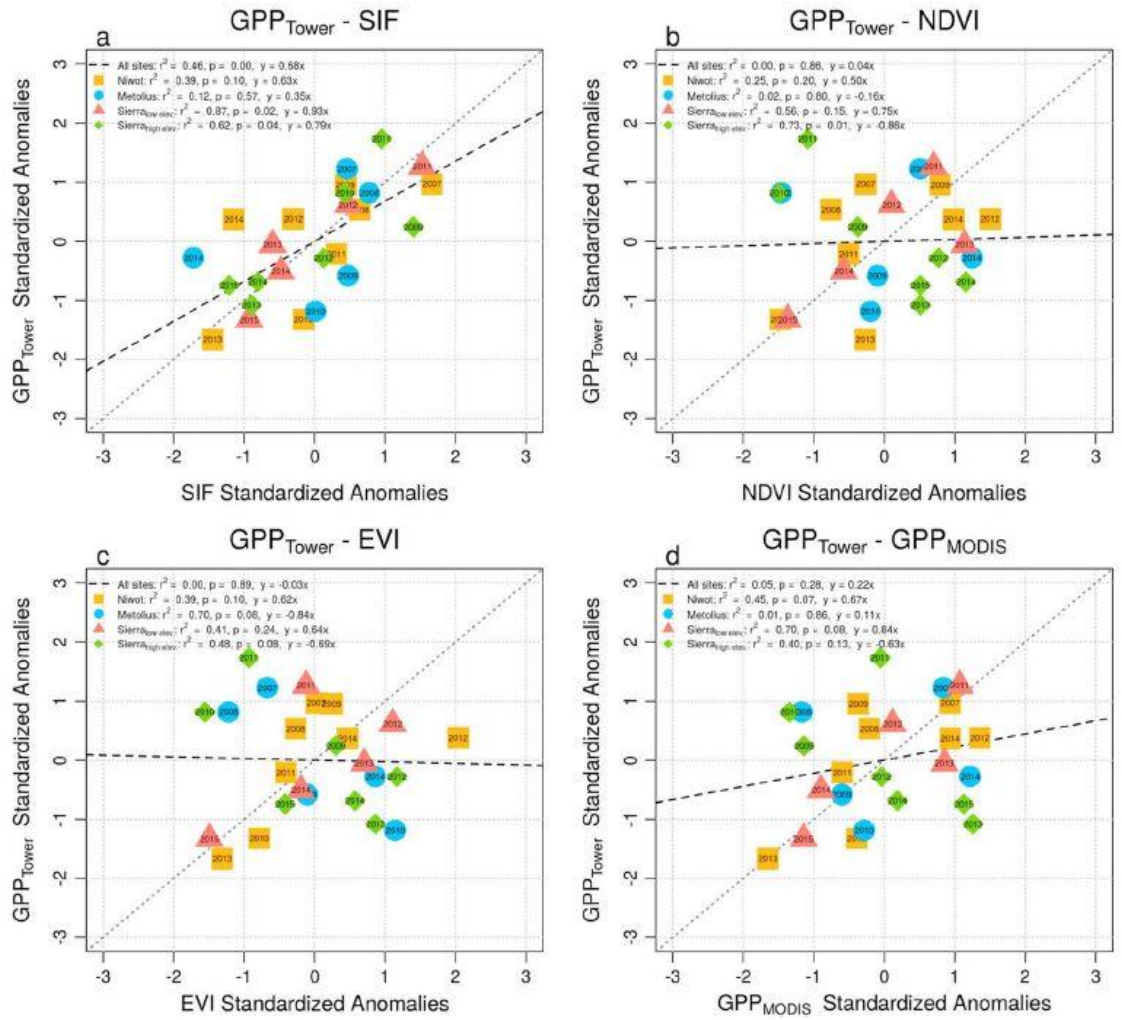

Figure 2. Scatter plots of GPP_{Tower} annual standardized anomalies compared to those for SIF (a), NDVI (weighted by solar radiation) (b), EVI (weighted by solar radiation) (c), and GPP_{MODIS} (d). The symbols are coded in both color and shape, with years indicated on the symbol. Site level r^2 values and p values are indicated next to the site name. The multisite r^2 and p values are also specified, with a corresponding linear regression, indicated by a dashed line. A 1:1 dotted line is shown for reference. Scatter plots for nonstandardized variables are shown for comparison in Figure S5. GPP = gross primary production; SIF = solar-induced chlorophyll fluorescence; NDVI = normalized difference vegetation index; EVI = enhanced vegetation index.

This paper compared Flux GPP and Satellite SiF (GOME-2). I think this is not that interesting result high relationship between GPP and SiF. In addtion, there should be limitation. The author also mentioned this limitation in this paper. 1) Foot print error between field observation and satellite. 2) Mixed biome in satellite image. 3) The satellite sensor degradation. To solve or reduce this limitation, we need field observation SIF data in coniferous forest site. In addtion, this paper shows the field observation in our coniferous site has potential opportunity to write paper such as comparison between SIF, VIs and GPP.

2nd August

Jia, M. et al., 2018. Difference and Potential of the Upward and Downward Sun-Induced Chlorophyll Fluorescence on Detecting Leaf Nitrogen Concentration in Wheat. Remote Sensing, 10(8): 1315.

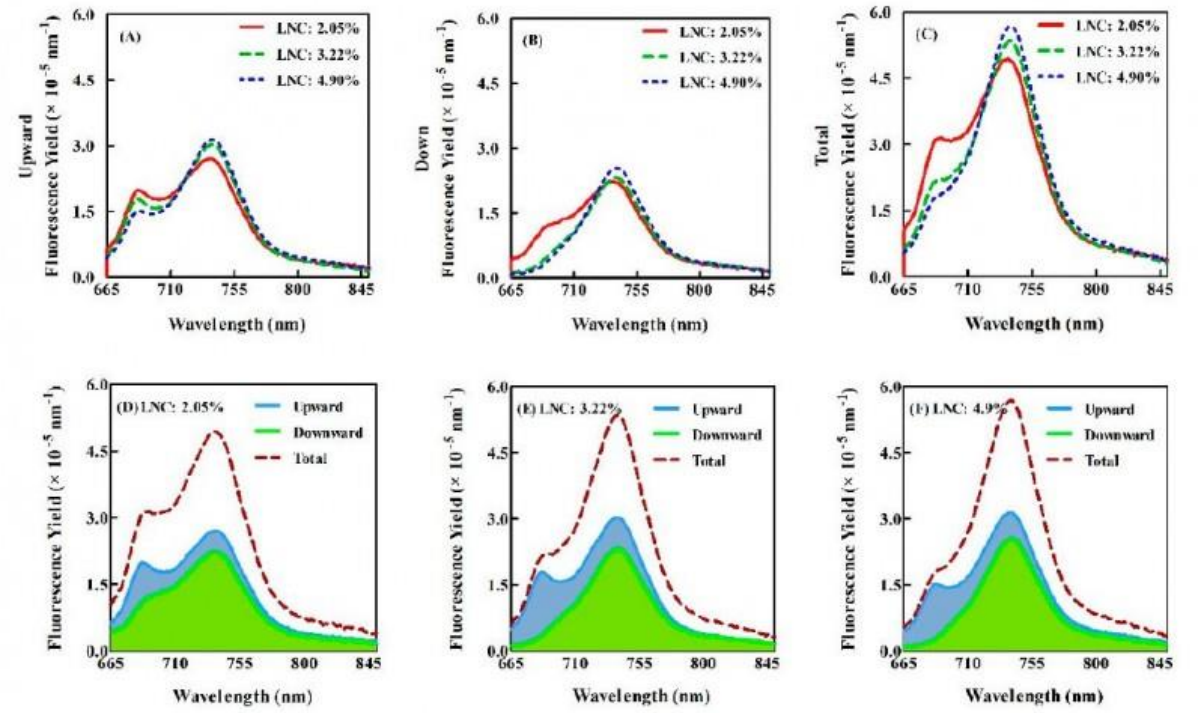

Figure 4. The upward, downward and total SIF yield spectra under different nitrogen levels in Experiment 2. Top row, each figure comparing different LNC contents for a given SIF component (**A**–**C**). Bottom row, each figure comparing the different SIF contributions for a given LNC (**D**–**F**).

In this paper, the author used Fluowat and ASD to extract SiF signal at upward and downward of leaves. I really want to know why the downward SiF signal is important for detecting leaf nitrogen. I think it is really hard to measure downward SiF signal in the field (I think upward also really painful) and I think already that many previous papers said there is a high relationship between nitrogen and spectral data. Although the reason why I choose this paper is this paper shows downward SiF signal and this paper shows there are many difference SIF curve within nitrogen.

1st August

Bonney, M. (2017). *Landscape variability of vegetation change across the forest to tundra transition of central Canada* (Doctoral dissertation).

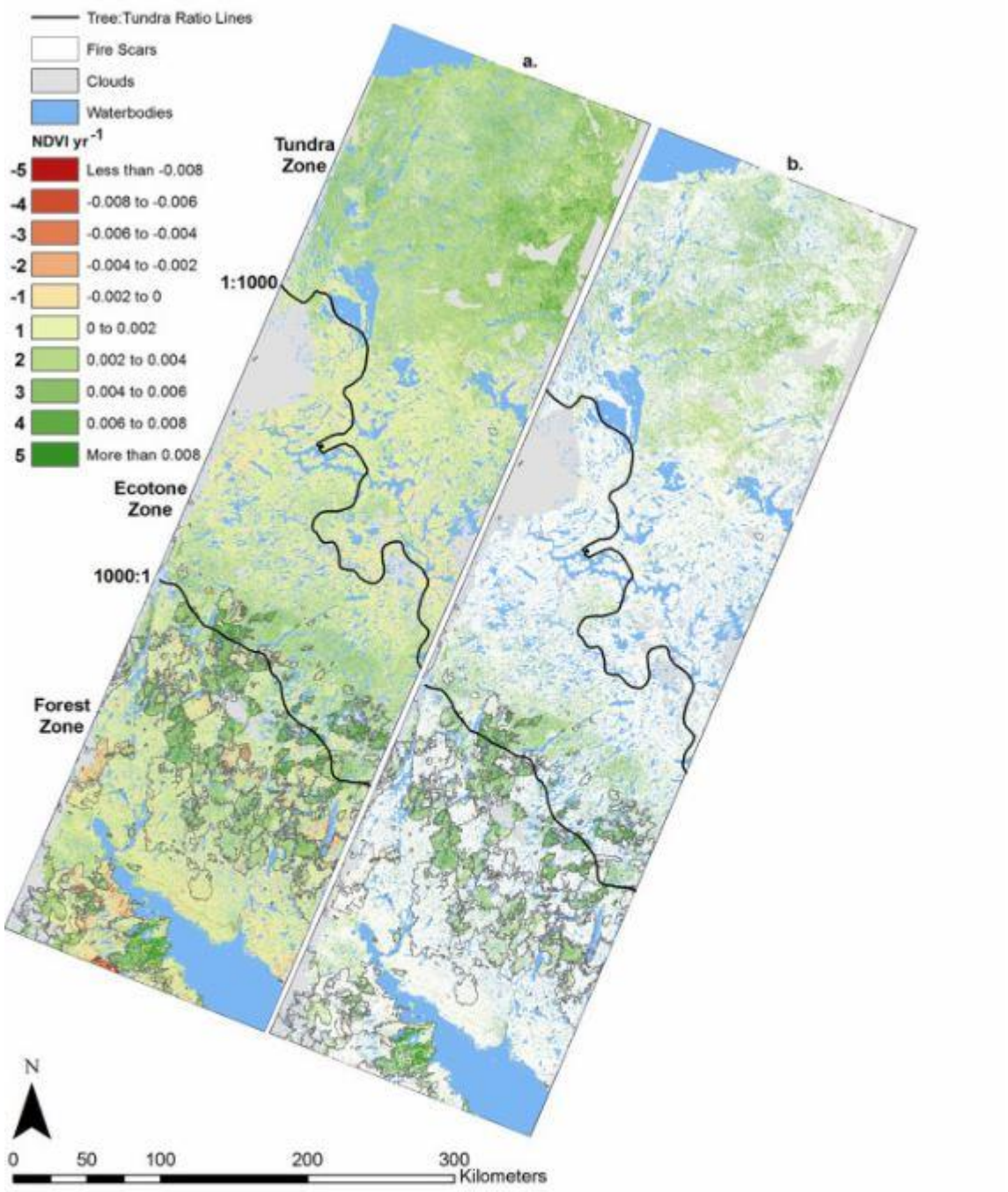

Download high-res image (1MB) Download full-size image

Fig. 5. Landsat NDVI trends (1984–2016) for the study area as determined using ordinary least squares regression. (a) All trends. (b) Significant ($p < 0.05$) trends only. Trends were binned into 10 levels for visualization purposes (−5 = most negative, 5 = most positive). Burned areas, waterbodies and cloudy areas were removed from analysis.

I think this paper is useful to write K-C project paper. This study used 33-year Landsat NDVI time series. 25% of the study area experienced greening, particularly at higher latitudes. In addition, non-tree vegetation volume measurements had a

strong relationship with NDVI. Dense shrublands and open woodlands showed the highest levels of greening.

4th July

Vrieling, A., Meroni, M., Darvishzadeh, R., Skidmore, A. K., Wang, T., Zurita-Milla, R., ... & Paganini, M. (2018). Vegetation phenology from Sentinel-2 and field cameras for a Dutch barrier island. *Remote sensing of environment*.

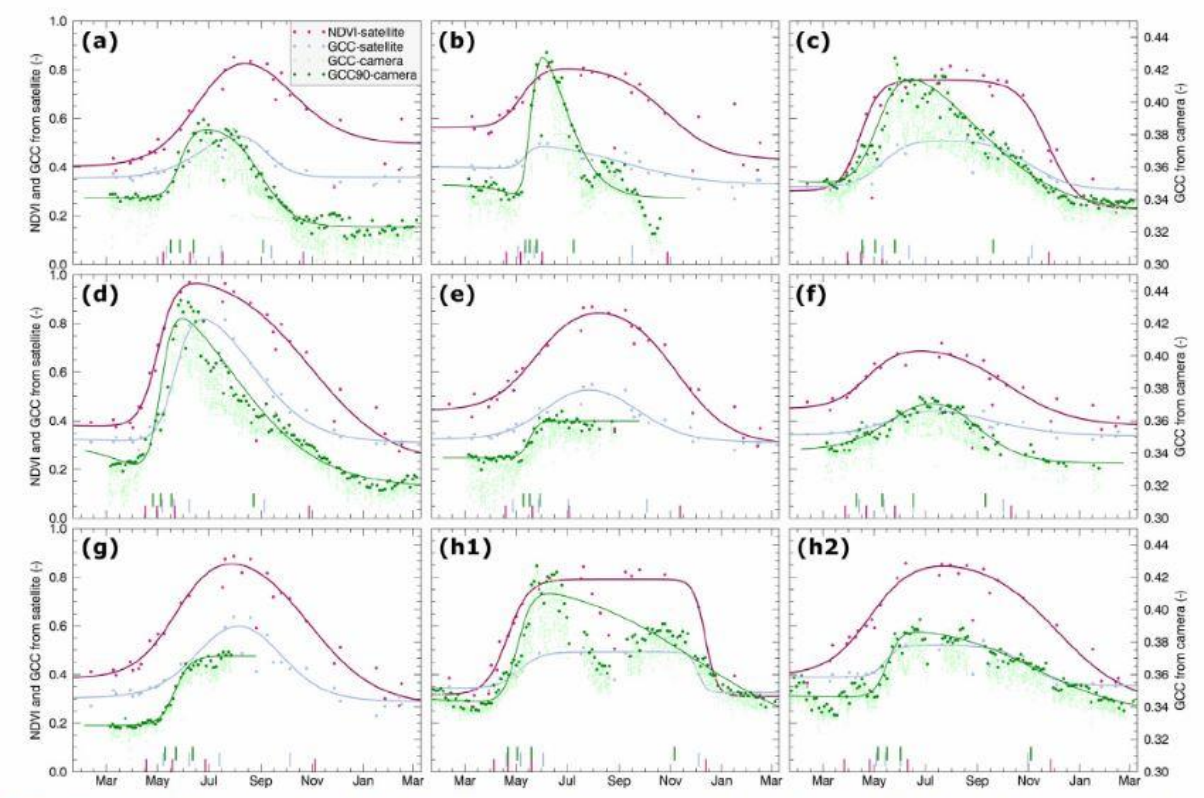

Fig. 3. Time series of $NDVI_s$ and GCC_s derived from Sentinel-2A, and GCC_c and $GCC90_c$ derived from the field cameras. Each panel relates to the corresponding camera identifier. For camera H two areas of interest are defined, corresponding to panels h1 and h2 in this figure. The fitted double hyperbolic tangent functions are plotted for each series (single for camera series E and G), and the corresponding retrievals for SOS_{20}, SOS_{50}, PS_{90}, and EOS_{50} are indicated as vertical lines at the bottom of each panel.

This paper found that Eos estimates from camera GCC series were on average almost two months before NDVI-based estimates. They said this could partially be explained by the observed exponential relationship between GCC and NDVI, as well as by the combined effect of viewing angle differences and the presence of non-photosynthetic elements in the vegetation canopy. A two-layer canopy radiative transfer model incorporating reduced chlorophyll levels in the upper layer provides a physically-based explanation of the viewing angle effect.

3rd July

Wang, M., Wu, J., Lafleur, P. M., Luan, J., Chen, H., & Zhu, X. (2018). Temporal shifts in controls over methane emissions from a boreal bog. *Agricultural and Forest Meteorology*, *262*, 120-134.

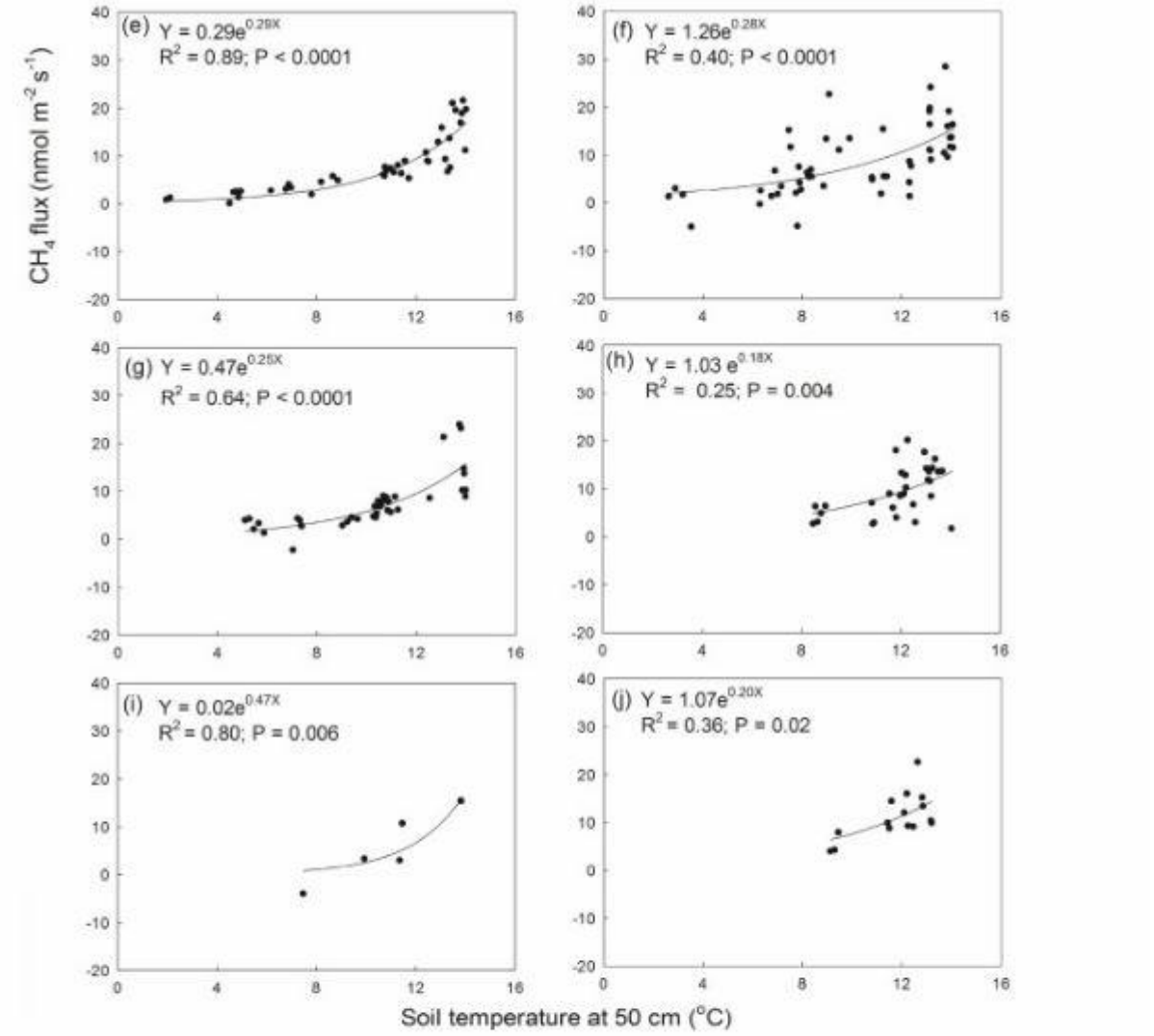

Download high-res image (539KB) Download full-size image

Fig. 6. The relationship between soil temperature at 50 cm and growing season CH_4 flux under different water table (WT) conditions. The left panel is for 2014 and the right one is for 2015. The panels from the top to the bottom were for WT range of -0.1 to -0.15 m (a, b), -0.15~-0.2 m (c, d), -0.2~-0.25 m (e, f), -0.25~-0.30 m (g, h) and -0.30 to -0.35 m (i,j), respectively.

Our lab also has measured CH4, so I have curious about it. This paper found that soil temperature at 50 cm and water table exerted interactive effects on CH4 flux and the non-growing season CH4 emissions accounted for ~ 40% of the annual emissions. I am curious that 50 cm temperature also affect CH4 flux in the rice paddy, which is charged by water.

2nd July

Guanter, L., Rossini, M., Colombo, R., Meroni, M., Frankenberg, C., Lee, J. E., & Joiner, J. (2013). Using field spectroscopy to assess the potential of statistical approaches for the retrieval of sun-induced chlorophyll fluorescence from ground and space. *Remote Sensing of Environment*, *133*, 52-61.

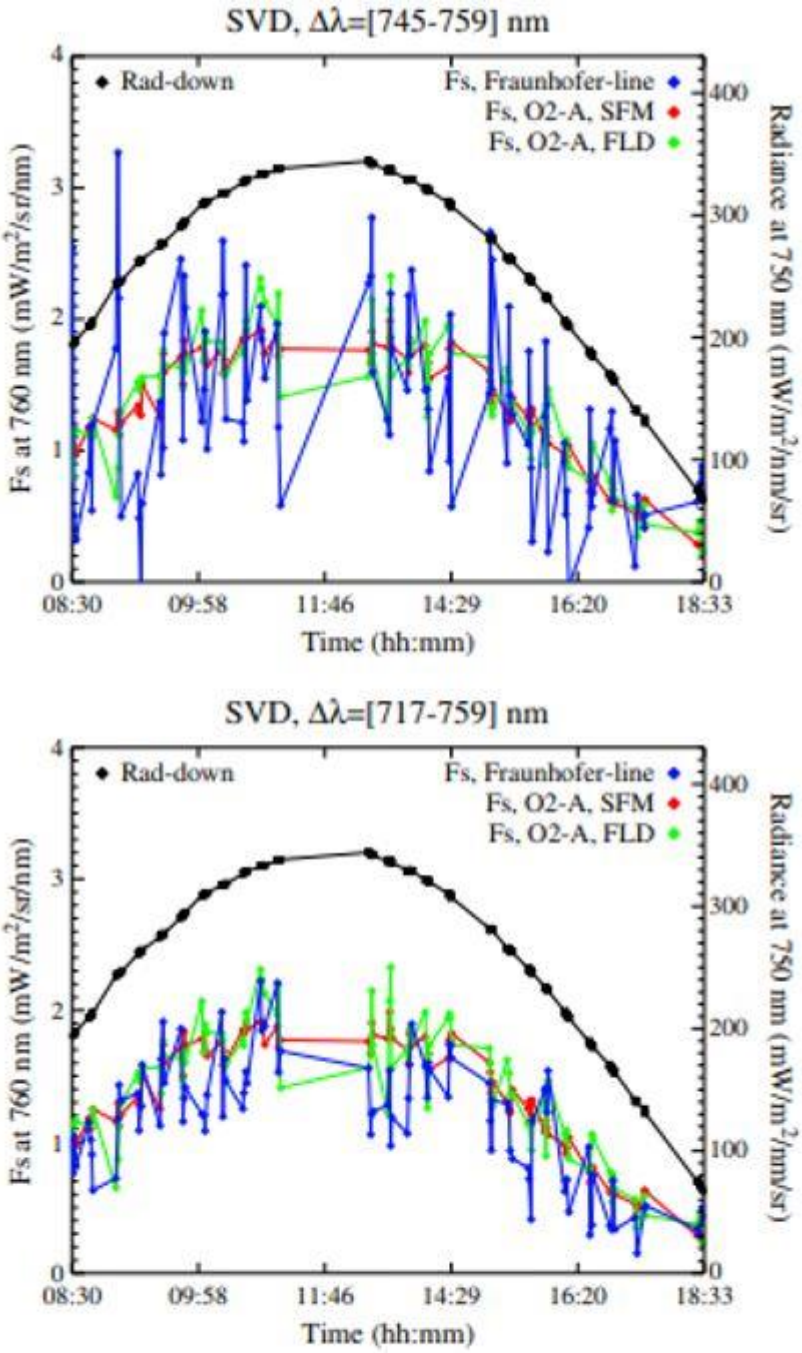

Fig. 8. Diurnal cycle of F_s on DOY 208 as calculated from the O_2A-band with FLD and SFM techniques and the SVD-based approach in 745–759 nm and 717–759 nm. The diurnal cycle of the down-welling sky radiance is also plotted. Samples between 11:00 and 12:00 are missing because at that time was impossible to view the target from nadir without shadowing it with the measurement system.

This paper shows that the magnitude of SVD, FLD, and SFM are similar. However, I think if we measure the SiF by using irradiance, there should be the difference between them. I think that FLD and SFM should be affected by SZA and azimuth angle. I will see deeper.

1st July

Grossmann, K. et al., 2018. PhotoSpec: A new instrument to measure spatially distributed red and far-red Solar-Induced Chlorophyll Fluorescence. Remote Sensing of Environment, 216: 311-327.

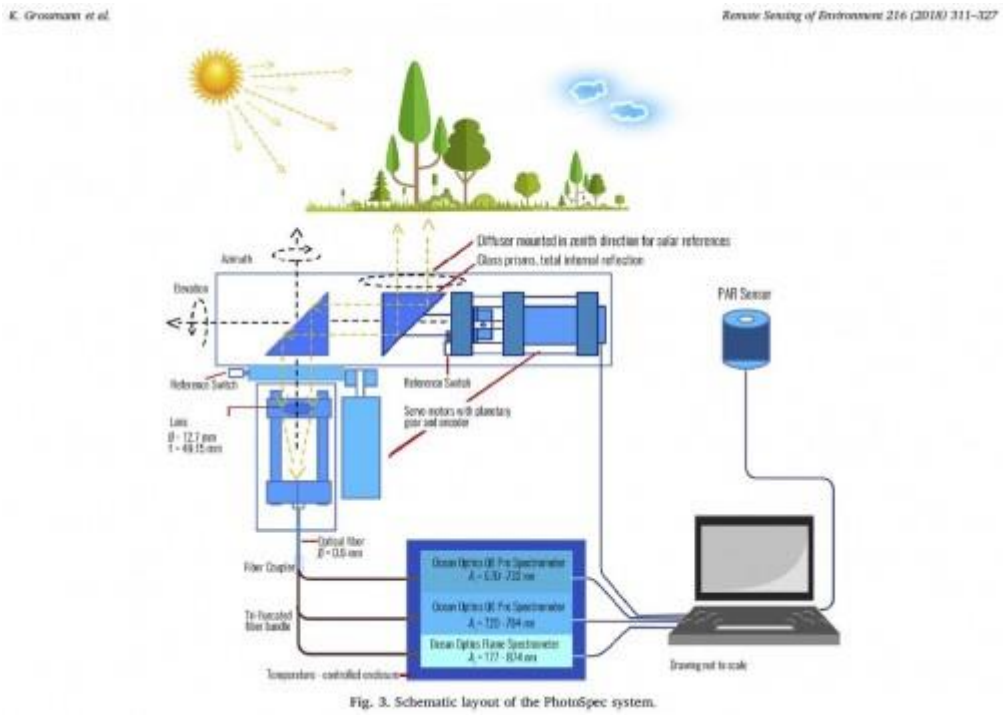

Fig. 3. Schematic layout of the PhotoSpec system.

This paper is very very interesting! I already saw the contents of this paper in last AGU. It is a really nice system. I think the advantage of this system is monitoring SiF with different FOV. For example, our SIF sensor and 4S-SIF only could measure the diffused light, so we could not distinguish where is the signal comes from. However, this system has three spectrometers and fiber system which could have possible the wavelength shifting.

4th June

Zhang, Y., Guanter**, L., Berry, J. A., Joiner, J., van der Tol, C., Huete, A., ... & Köhler, P. (2014). Estimation of vegetation photosynthetic capacity from space-based measurements of chlorophyll fluorescence for terrestrial biosphere models. *Global Change Biology*, *20*(12), 3727-3742.**

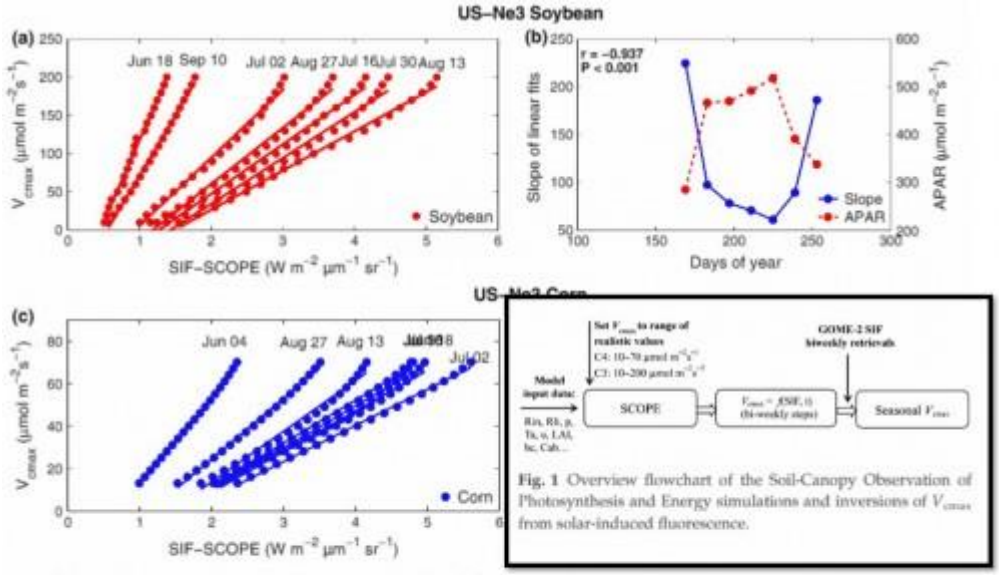

Fig. 3 Relationship between biweekly V_{cmax} and solar-induced fluorescence from Soil-Canopy Observation of Photosynthesis and Energy simulations for soybean (a) and corn (c) years at the US Ne3 site. (b) and (d) are the slopes of the fits in (a) and (c) and the seasonal absorbed photosynthetic active radiation (APAR) during the growing season. Pearson product–moment correlations are shown between the slopes and APAR in (b) and (d). Each linear relationship represents a biweekly period during the growing season, e.g., the first left most line in (a) is for June 18–July 1 of 2008.

Fig. 1 Overview flowchart of the Soil-Canopy Observation of Photosynthesis and Energy simulations and inversions of V_{cmax} from solar-induced fluorescence.

This paper is very interesting! I am not sure the VCmax is relatived with SiF… I should study about that. I am not good at the modelling however, I think this method will be used to get SIF signal by using the process-based model.

3rd June

Magney, T. S., Eitel, J. U., Huggins, D. R., & Vierling, L. A. (2016). Proximal NDVI derived phenology improves in-season predictions of wheat quantity and quality. *Agricultural and Forest Meteorology*, *217*, 46-60.

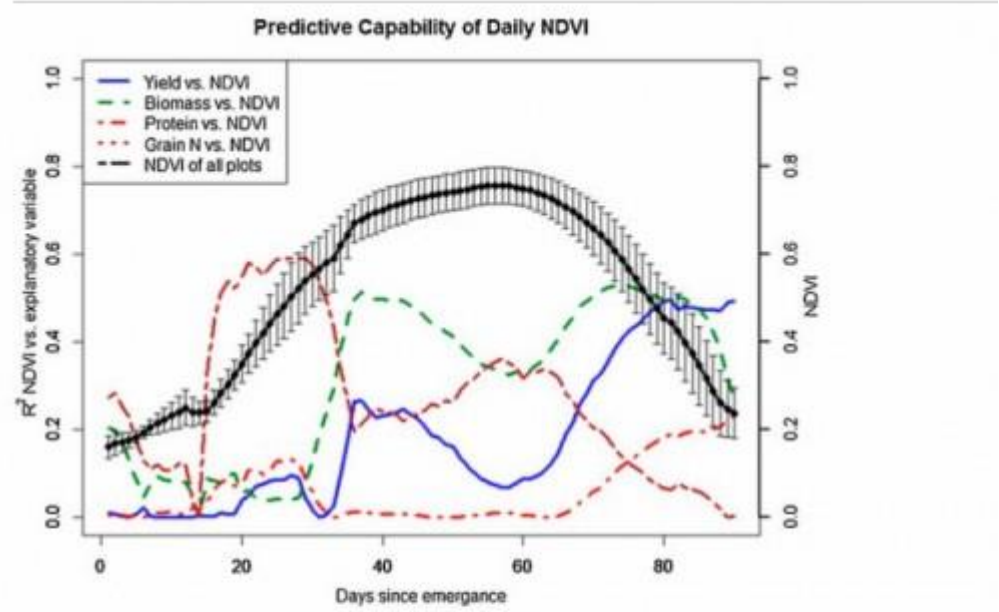

Download high-res image (428KB) Download full-size image

Fig. 3. Seasonal trend in the daily NDVI data values (black) with error bars representing 95% confidence intervals around daily NDVI data for all plots. All daily NDVI values were normalized to 'days since emergence' since the phenology varied from plot to plot depending on location and season. Individual daily NDVI data vs. end of season yield (blue), biomass (green), protein (red), and grain N (brown) coefficients of determination (R^2) are also plotted throughout the season (each model determined from n = 16). (For interpretation of the references to color in this figure legend, the reader is referred to the web version of this article.)

This paper by using automated sensors, which can provide information about crop development and performance across time. The author examined the hypothesis that ground-based canopy reflectance data might define crop phenology in new ways over the course of the season that can better forecast crop yield, protein, biomass, and grain nitrogen at harvest. This study examines the utility of daily Normalized Difference Vegetation Index (NDVI) data to monitor crop phenology over two complete growing seasons. I think 4S could be used for this kind of study.

2nd June

Baret, F., De Solan, B., Lopez-Lozano, R., Ma, K., & Weiss, M. (2010). GAI estimates of row crops from downward looking digital photos taken perpendicular to rows at 57.5 zenith angle: Theoretical considerations based on 3D architecture models and application to wheat crops. ***Agricultural and Forest Meteorology*****,** ***150*****(11), 1393-1401.**

$$Po(57.5^\circ) = e^{0.5 \cdot LAI / \cos 57.5^\circ} \Leftrightarrow LAI = -\frac{\cos 57.5^\circ}{0.5} \log(Po(57.5^\circ)) \quad (1)$$

Note that in this case *LAI*, *PAI* and *GAI* are equivalent since only green leaves are represented.

2.2. Simulations based on the ADEL-wheat 3D architecture model of wheat crops

Adel-wheat (Fournier et al., 2003, Evers et al., 2007) is a dynamic architectural model of wheat, based on the L-system principles (Lindenmayer, 1968, Prusinkiewicz, 1999, Prusinkiewicz et al., 2000). From a given initial planting pattern of seeds, the model describes the size, shape, and orientation in space of each organ of a plant population as a function of degree days above 0 °C. The model was calibrated over several experiments. Some of the characteristics such as leaf blade curvature and orientation in space are drawn from experimental distribution laws (Fig. 2).

This paper already tried to estimate green leaf area index. However, I think the advantage of our method (camera GI + LED GF) is easier. This method requires the 3D model and I am not sure this method is working well in different view angle (not the camera, I mean the row of the canopy).

1st June

Hilton, T. W. (2018). Photosynthesis in high definition. *Nature Climate Change*, *8*(1), 20.

Once inside of the leaf, OCS is irreversibly destroyed by carbonic anhydrase, the same enzyme that separates CO2 into its constituent atoms. Observing ambient OCS concentrat, therefore,fore opens a window to view stomatal conductance, the acquisition of raw materials for photosynthesis from outside the leaf. Simultaneously constraining the ‘outside-of-leaf-cells’ stomatal conductance with OCS observations, and the ‘inside-of-leaf-cells’ photochemistry with SIF observations, uses two independent

---

4th May

Zhang, Y., Chen, J. M., & Miller, J. R. (2005). Determining digital hemispherical photograph exposure for leaf area index estimation. *Agricultural and Forest Meteorology*, *133*(1-4), 166-181.

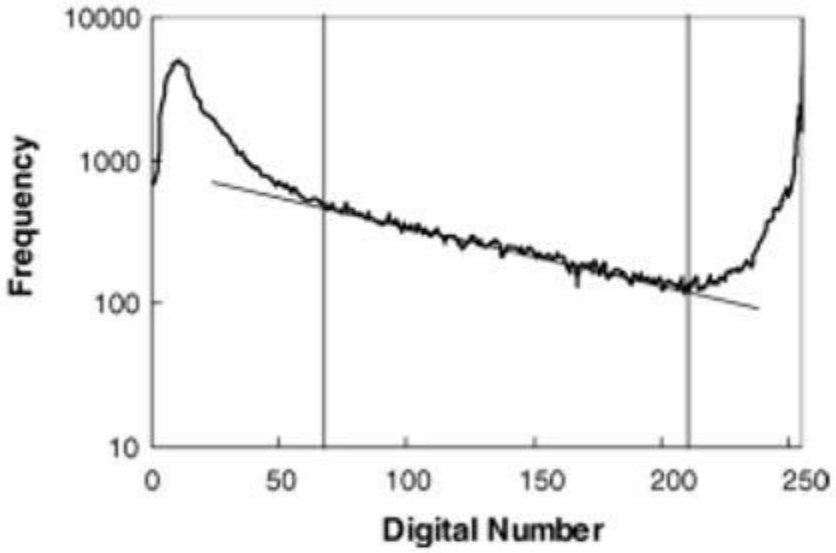

Fig. 2. Digital number histogram of a nine-degree annulus from a single digital hemispherical photograph. The *y*-axis is in a logarithm scale to demonstrate the mixed pixel part of the histogram found between the two thresholds (DN_{min} = 71, DN_{max} = 212). DN_{min} and DN_{max} are respectively determined where the linear part of the histogram in a logarithm starts and ends.

This paper is quite interesting. This paper developed the method, which can classify leaf and sky. However, this method showed that the relative exposure value affect the GF! This paper should be comparable to our Hwang's method.

3rd May

Cardona, T., Sedoud, A., Cox, N., & Rutherford, A. W. (2012). Charge separation in photosystem II: a comparative and evolutionary overview. *Biochimica et Biophysica Acta (BBA)-Bioenergetics*, *1817*(1), 26-43.

I have always question "why the leaves are green?" In the introduction of this paper, the author showed the answer.

"When chlorophyll absorbs light, an electron is promoted from the highest occupied molecular orbital to the lowest or second lowest unoccupied molecular orbital. The energy in red light corresponds to the transition up to the first excited singlet state. The greater energy in blue light is sufficient for the electron to reach the higher excited singlet state but this state decays rapidly, with the loss of some energy, to form the longer-lived, first excited state. Thus the energy available for photochemistry corresponds to that of the red photon (e.g. 680 nm=1.82 eV). The energy of green light does not correspond to that needed to promote, a valence

electron to an excited state and thus it is not absorbed but instead reflected or transmitted. Hence, chlorophyll is green."

2nd May

Han, T. H., & Kuo, Y. F. (2018). Developing a system for three-dimensional quantification of root traits of rice seedlings. *Computers and Electronics in Agriculture*, *152*, 90-100.

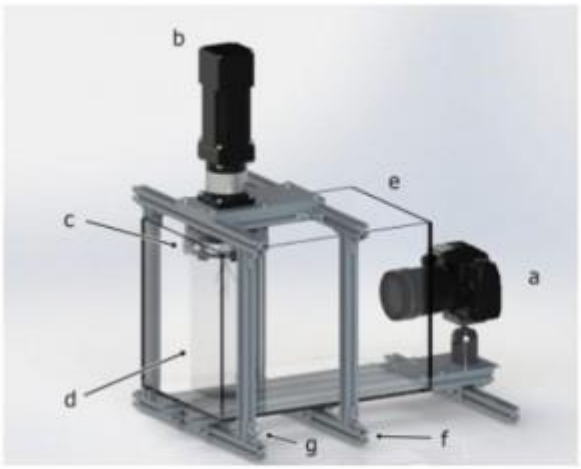

Download high-res image (102KB) Download full-size image

Fig. 3. Schematic of the imaging system: (a) digital camera, (b) servomotor, (c) connecter, (d) glass tube containing phytagel and the rice seedling, (e) water tank, (f) adjustable horizontal stand, and (g) LED illuminator.

This paper quite interesting about how can we measure the root area. I think this method could be used to measure root weight or area for CCS project.

1st May

Lubitz, W., Reijerse, E. J., & Messinger, J. (2008). Solar water-splitting into H 2 and O 2: design principles of photosystem II and hydrogenases. *Energy & Environmental Science*, *1*(1), 15-31.

This paper is one of the key paper about SiF and water oxidation. " PS2, therefore, requires protection, for example against oxidation or long-lived triplet states, Chl, that can form by charge recombination reactions." This defence system is relative to the SIF.

$$Chl_A^* \; Chl_{RC} \; Pheo \rightarrow Chl_A \; Chl_{RC}^* \; Pheo \rightarrow Chl_A \; Chl_{RC}^{\bullet+} \; Pheo^{\bullet-}. \quad (4)$$

The radical cation $Chl_{RC}^{\bullet+}$, also known by the absorption maximum of Chl_{RC} as $P680^{\bullet+}$, has an estimated oxidizing potential of +1.2 to 1.3 V, the highest known in biology.[40] PSII therefore requires protection, for example against oxidation or long lived triplet states, ^3Chl, that can form by charge recombination reactions. The two carotenoid molecules, Car, (Fig. 2B) and the cyt *b*559 (Fig. 2A and B) are believed to be involved in this defense system. The primary charge separation is stabilized by electron transfer from $Pheo^{\bullet-}$ to the bound plastoquinone (PQ) molecule Q_A, and by the reduction of $P680^{\bullet+}$ by a redox active tyrosine side chain of the D1 protein, Y_Z. These electron transfer reactions increase the distance between the charged species and decrease the energy difference ΔG. Both factors

---

4th April

Sun, Y., Frankenberg, C., Wood, J. D., Schimel, D. S., Jung, M., Guanter, L., ... & Gu, L. (2017). OCO-2 advances photosynthesis observation from space via solar-induced chlorophyll fluorescence. *Science*, *358*(6360), eaam5747.

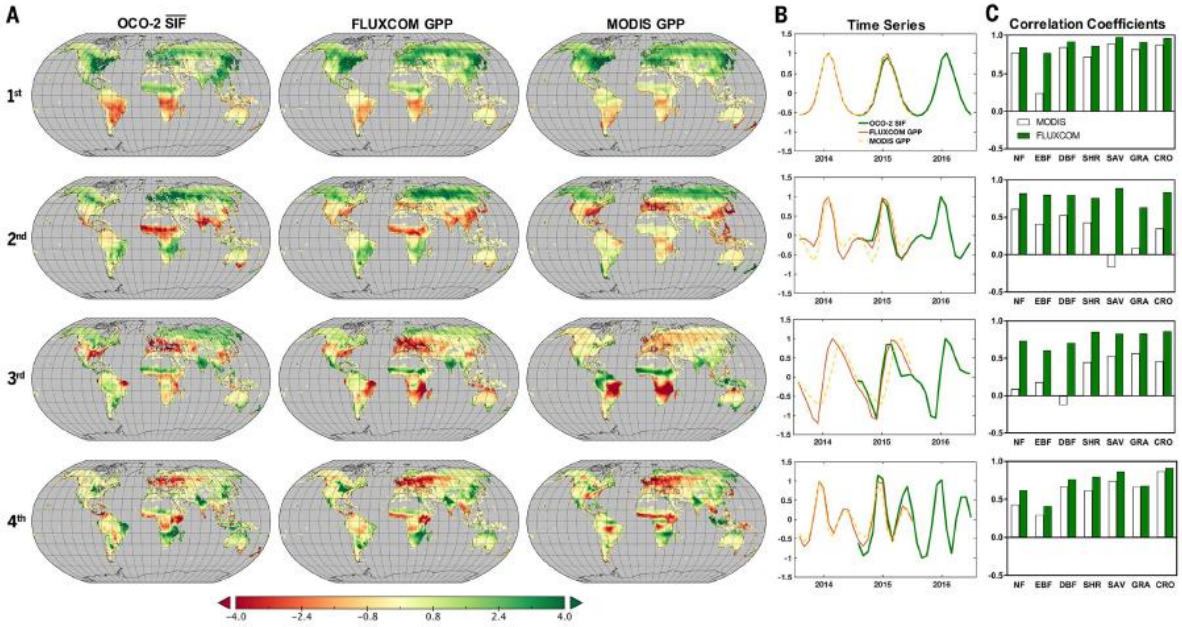

Fig. 4. Spatiotemporal patterns of EOF decomposition of OCO-2 $\overline{SIF}$, FLUXCOM GPP, and MODIS GPP for the first four leading modes in descending order. (**A**) Spatial maps of EOFs from monthly data sets. (**B**) Corresponding time series of each EOF. (**C**) Quantification of the spatial resemblance of OCO-2 $\overline{SIF}$ with FLUXCOM (green) and MODIS GPP (white) across biomes, denoted as NF (needleleaf forests), EBF (evergreen broadleaf forests), DBF (deciduous broadleaf forests), SHR (shrublands), SAV (savannas), GRA (grasslands), and CRO (croplands). The land cover data are from the International Satellite Land Surface Climatology Project Initiative II biome classification products using the International Geosphere-Biosphere Programme (IGBP) scheme, following (*11*).

This paper showed that OCO-2 represents a major advance in satellite SiF remote sensing. They suggested that SiF is a powerful proxy for GPP at multiple spatiotemporal scales and that high-quality satellite SiF is of central importance to studying terrestrial ecosystems and the carbon cycle.

I have questions about this figure. What is the meaning that the number of figure caption? Such as 1st 2nd..? And why the relationship is quite poor at 2nd and 3rd in needle leaf forest site?

3rd April

Sun, Y., Frankenberg, C., Jung, M., Joiner, J., Guanter, L., Köhler, P., & Magney, T. (2018). Overview of Solar-Induced chlorophyll Fluorescence (SIF) from the Orbiting Carbon Observatory-2: Retrieval, cross-mission comparison, and global monitoring for GPP. Remote Sensing of Environment, 209, 808-823c

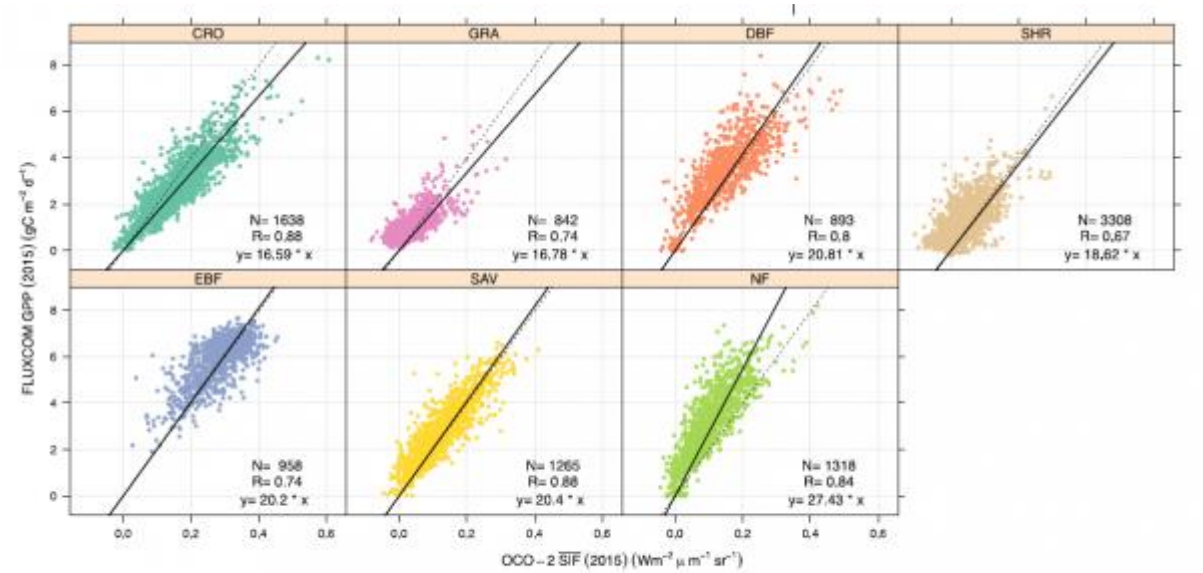

Fig. 12. The relationships between the annual mean OCO-2 SIF and FLUXCOM GPP in 2015 for different biomes. Each scatter represents a grid-cell. The fitted linear regression lines passing through the origin are displayed (solid), along with the regression line fitted with all biomes (dotted). The ordinary least square (OLS) regression is used here for the fitting. Biomes are denoted as: CRO for croplands, GRA for grasslands, DBF for deciduous broadleaf forests, SHR for shrublands, EBF for evergreen broadleaf forests, SAV for savannas, NF for needleleaf forests, respectively.

This paper really well organizes the difference between OCO-2, GOME2, GOSAT. In addition, this paper showed the linear relationship between satellite SiF and GPP. The linear relationship between OCO-2 SIF and existing modeled GPP products diverges somewhat across biomes at the global scale, consistent with previous GOSAT or GOME-2 based findings when modeled GPP products were used, but in contrast to a consistent cross-biome SIF-GPP relationship obtained at flux tower sites with OCO-2 products. This contrast suggests a critical need to reconcile differences in diverse SIF and GPP products and the relationships among them.

2nd Aprl

Miao, G., Guan, K., Yang, X., Bernacchi, C. J., Berry, J. A., DeLucia, E. H., ... & Peng, B. (2018). Sun-Induced Chlorophyll Fluorescence, Photosynthesis, and Light Use Efficiency of a Soybean Field from Seasonally Continuous Measurements. *Journal of Geophysical Research: Biogeosciences*, *123*(2), 610-623.

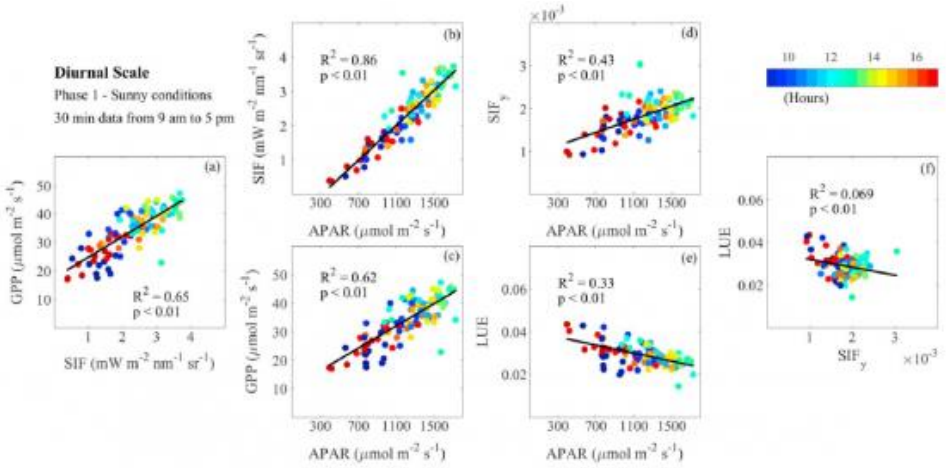

Figure 5. Relationships based on the 30 min data at the soybean field under sunny conditions at Phase 1 (both canopy structure and physiological status were relatively stable): (a) gross primary productivity (GPP):Sun-induced chlorophyll fluorescence (SIF), (b) SIF:absorbed photosynthetically active radiation (APAR), (c) GPP: APAR, (d) Sun-induced chlorophyll fluorescence yield (SIF_y):APAR, (e) light use efficiency (LUE):APAR, and (f) LUE:SIF_y. The color scheme represents the time stamps at 30 min interval from 9 to 17. A linear regression between the paired variables is applied when such a relationship is statistically significant ($p < 0.01$).

I think this paper also quite similar to our result. However, this paper also showed linearity between PAR and GPP is better than SiF and GPP. Then why should we use the SiF? I think there should be some reason.

1st April

Baker, N. R. (2008). Chlorophyll fluorescence: a probe of photosynthesis in vivo. *Annu. Rev. Plant Biol.*, *59*, 89-113.

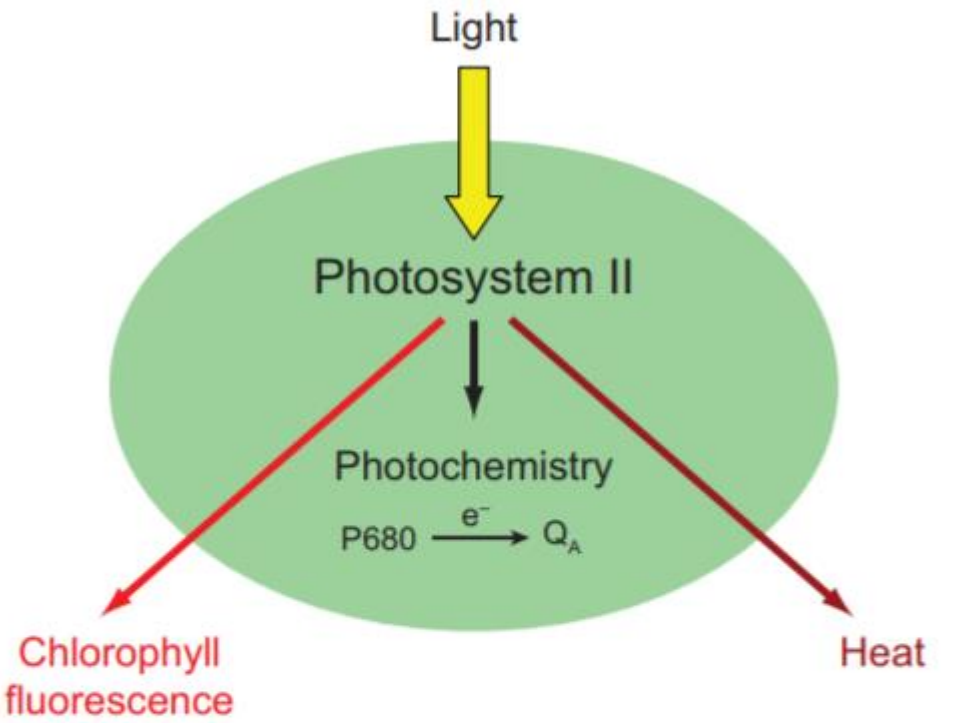

Figure 1

Simple model of the possible fate of light energy absorbed by photosystem II (PSII). Light energy absorbed by chlorophylls associated with PSII can be used to drive photochemistry in which an electron (e^-) is transferred from the reaction center chlorophyll, P680, to the primary quinone acceptor of PSII, Q_A. Alternatively, absorbed light energy can be lost from PSII as chlorophyll fluorescence or heat. The processes of photochemistry, chlorophyll fluorescence, and heat loss are in direct competition for excitation energy. If the rate of one process increases the rates of the other two will decrease.

One of the key paper about SiF. consideration is given to problems associated with accurate estimation of the PSII operating efficiency measured by fluorescence and its relationship with the rates of linear electron flux and CO2 assimilation. The roles of photochemical and nonphotochemical quenching in the determination of changes in PSII operating efficiency are examined.

4th March

Kirby, J., Chapman, L., & Chapman, V. (2018). Assessing the Raspberry Pi as a low-cost alternative for acquisition of near infrared hemispherical digital imagery. *Agricultural and Forest Meteorology*, *259*, 232-239.

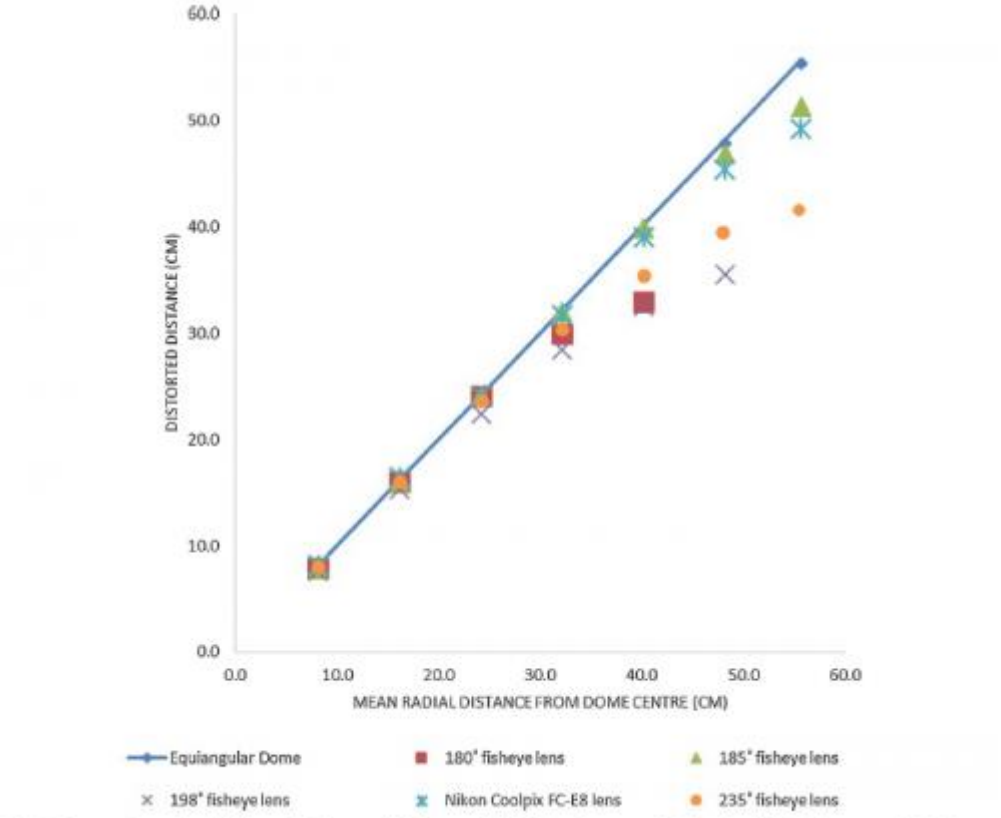

Fig. 3. Comparison of radial distortion between different mobile fisheye lenses and Nikon Coolpix 4500 camera FC-E8 lens.

I found a quite interesting paper about a camera. this paper conducts a comparison between a Nikon Coolpix camera and a cheaper alternative, the Raspberry Pi NoIR camera, to assess its suitability as a viable alternative for future research. The results are promising with low levels of distortion, comparable to the Nikon. Resultant sky-view factor analyses also yield encouraging results, but challenges remain to overcome small differences in the field of view as well as improving the present availability of bespoke fittings.

3rd March

Huete, A., Didan, K., Miura, T., Rodriguez, E. P., Gao, X., & Ferreira, L. G. (2002). Overview of the radiometric and biophysical performance of the MODIS vegetation indices. *Remote sensing of environment*, *83*(1-2), 195-213.

$$EVI = G \frac{\rho_{NIR} - \rho_{red}}{\rho_{NIR} + C_1 \times \rho_{red} - C_2 \times \rho_{blue} + L} \quad (2)$$

where ρ are atmospherically corrected or partially atmosphere corrected (Rayleigh and ozone absorption) surface reflectances, L is the canopy background adjustment that addresses nonlinear, differential NIR and red radiant transfer through a canopy, and C_1, C_2 are the coefficients of the aerosol resistance term, which uses the blue band to correct for aerosol influences in the red band. The coefficients adopted in the EVI algorithm are, $L = 1$, $C_1 = 6$, $C_2 = 7.5$, and G (gain factor) = 2.5 (Huete, Justice, & Liu, 1994; Huete, Liu, Batchily, & van Leeuwen, 1997).

This is key paper about MODIS VI such as NDVI and EVI. I have question about how they provide MODIS NDVI and EVI with in multiple-days. In this paper shows the way to process. In addition, this paper mention how to calculate parameter for EVI processing.

_ BRDF-C: bidirectional reflectance distribution function composite,

_ CV-MVC: constrained-view angle-maximum value composite,

_ MVC: maximum value composite.

2nd March

Rossini, M., Meroni, M., Celesti, **M., Cogliati, S., Julitta, T., Panigada, C., ... & Colombo, R. (2016). Analysis of red and far-red sun-induced chlorophyll fluorescence and their ratio in different canopies based on observed and modeled data.** ***Remote sensing*****, *8*(5), 412.**

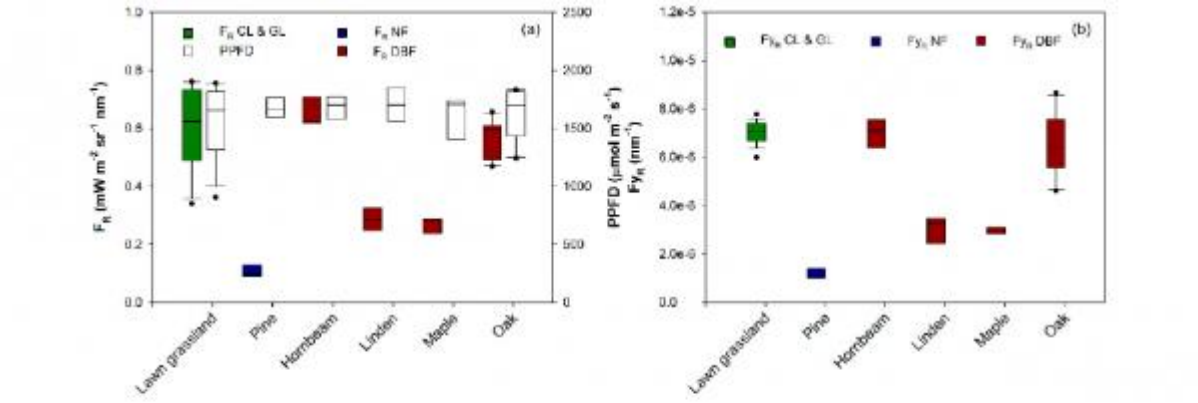

Figure 2. (**a**) Plot of the median, 10th, 25th, 75th and 90th percentiles as vertical boxes of the F; and (**b**) apparent fluorescence yield in the O_2-B band for different species. Full bars refer to F and Fy estimation, while empty bars refer to the incident photosynthetic photon flux density (PPFD) expressed in $\mu mol \cdot m^{-2} \cdot s^{-1}$. The statistics refer to 20 samples for each species. CL: cropland, GL: grassland, NF: Needleleaf Forest, DBF: Deciduous Broadleaf Forest.

I think I should study Soil-Canopy Observation of Photochemistry and Energy fluxes (SCOPE) model to master SiF. simulation results confirmed a major contribution of leaf chlorophyll concentration and LAI to the fluorescence signal. However, some discrepancies between simulated and experimental data were found in broadleaf species. These discrepancies may be explained by uncertainties in individual species LAI estimation in mixed forests or by the effect of other model parameters and/or model representation errors. This is the first study showing sun-induced fluorescence experimental data on the variations in the two emission regions and providing quantitative information about the absolute magnitude of fluorescence emission from a range of vegetation types.

1st March

Julitta, T., Rossini, M., Burkart, A., Cogliati, S., Davies, N., Hom, M., ... & Colombo, R. (2016). Comparison of sun-induced chlorophyll fluorescence estimates obtained from four portable field spectroradiometers. *Remote Sensing*, *8*(2), 122.

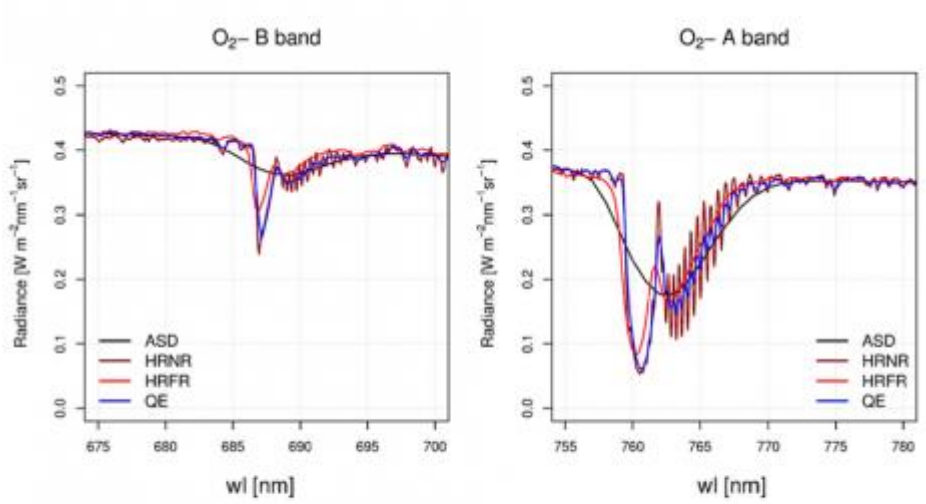

Figure 2. Incoming radiance measured with the four spectroradiometers in the O_2-B band (**left**) and in the O_2-A band (**right**). Each color represents a different instrument. The ability to detect the presence of narrow absorption features is directly related to the Spectral Resolution (*i.e.*, FWHM) of each device.

When I tried to get linear response curve between QEpro, ASD and Filter based SiF sensor, the linearity was quite weird. I suspect the reason that it comes from resolution between sensors. This paper compared within different resolution spectrometer. This paper showed the SNR and resolution is very important to get SiF signal.

4th Feb

Yang, H., Yang, X., Zhang, Y., Heskel, M. A., Lu, X., Munger, J. W., ... & Tang, J. (2017). Chlorophyll fluorescence tracks seasonal variations of photosynthesis from leaf to canopy in a temperate forest. *Global change biology*, *23*(7), 2874-2886.

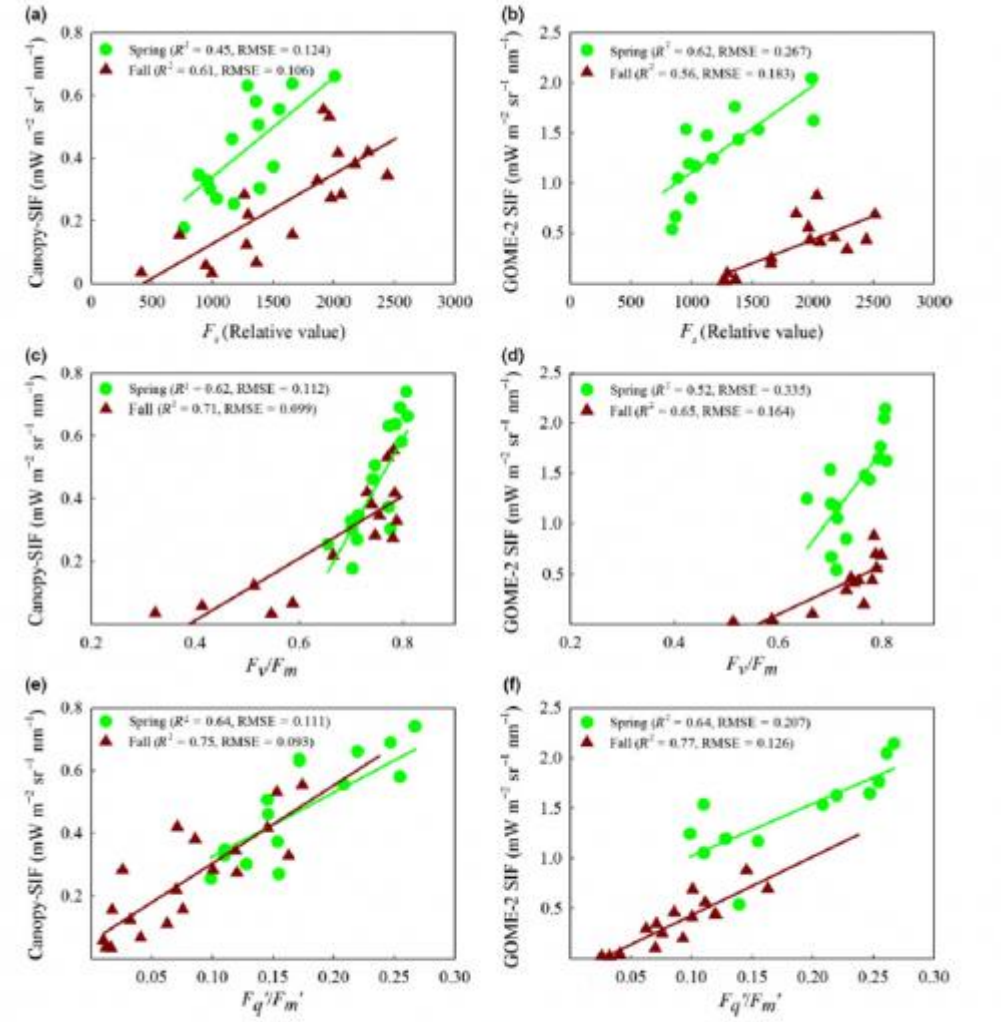

Fig. 2 The seasonal relationships between daily mean leaf-scaled fluorescence parameters and upscaled SIF. (a, b) Linear relationships between leaf-scaled steady-state fluorescence (F_s) and canopy-SIF and GOME-2 SIF, respectively; (c, d) linear relationships between leaf-scaled F_v/F_m and canopy-SIF and GOME-2 SIF, respectively; (e, f) linear relationships between leaf-scaled F_q'/F_m' and canopy-SIF and GOME-2 SIF, respectively. [Colour figure can be viewed at wileyonlinelibrary.com]

This paper linked at different spatial scales across the growing season. The author examined seasonal relationships between ChlF and photosynthesis at the leaf, canopy and ecosystem scales and explored how leaf-level ChlF was linked with canopy-scale SiF in deciduous forest. It is quite interesting paper because scale up is really hard (footprint, time scale, sampling method..) This result suggest that ChlF can be a powerful tool to track photosynthesic rates at leaf, canopy and ecosystem scales.

3rd Feb

Runkle, B. R. K., Sachs, T., Wille, C., Pfeiffer, E. M., & Kutzbach, L. (2013). Bulk partitioning the growing season net ecosystem exchange of CO 2 in Siberian tundra reveals the seasonality of its carbon sequestration strength. *Biogeosciences*, *10*(3), 1337-1349.

$$F_{CO_2} = \text{NEE} = P_{\text{gross},2} + R_{\text{eco},2} = -\frac{P_{\text{max},2}\alpha_2 \text{PAR}}{P_{\text{max},2} + \alpha_2 \text{PAR}} + R_{\text{base},2} Q_{10,2}^{\frac{T_s - T_{\text{ref}}}{\gamma}}.$$

The NEE time series is then partitioned in 7-day inter
using $R_{\text{base},2}$ and $Q_{10,2}$ to estimate $R_{\text{eco},2}$ and setting
residual flux to $P_{\text{gross},2}$. This derived P_{gross} flux term is t
modelled by refitting a light-response curve across the wl
range of incoming PAR using a new pair of positive-val
parameters, α_3 and $P_{\text{max},3}$:

$$P_{\text{gross},2} = \text{NEE} - R_{\text{base},2} Q_{10,2}^{\frac{T_s - T_{\text{ref}}}{\gamma}} = -\frac{P_{\text{max},3}\alpha_3 \text{PAR}}{P_{\text{max},3} + \alpha_3 \text{PAR}}.$$

I always curious about how can we divide respiration and photosynthesis in tundra or taiga site because there is no sunset in the artic site to calculate respiration in dark time. In this paper, the authors used PAR and Q10 to dived respiration and exchange of Co2. I think this paper also used an arbitrary threshold to determine when is starting respiration using PAR. I hope if the SiF sensor is working well, I will be useful in the artic site.

2nd Feb

Hasegawa, K., Izumi, T., Matsuyama, H., Kajiwara, K., & Honda, Y. (2018). Seasonal change of bidirectional reflectance distribution function in mature Japanese larch forests and their phenology at the foot of Mt. Yatsugatake, central Japan. *Remote Sensing of Environment*, *209*, 524-539.

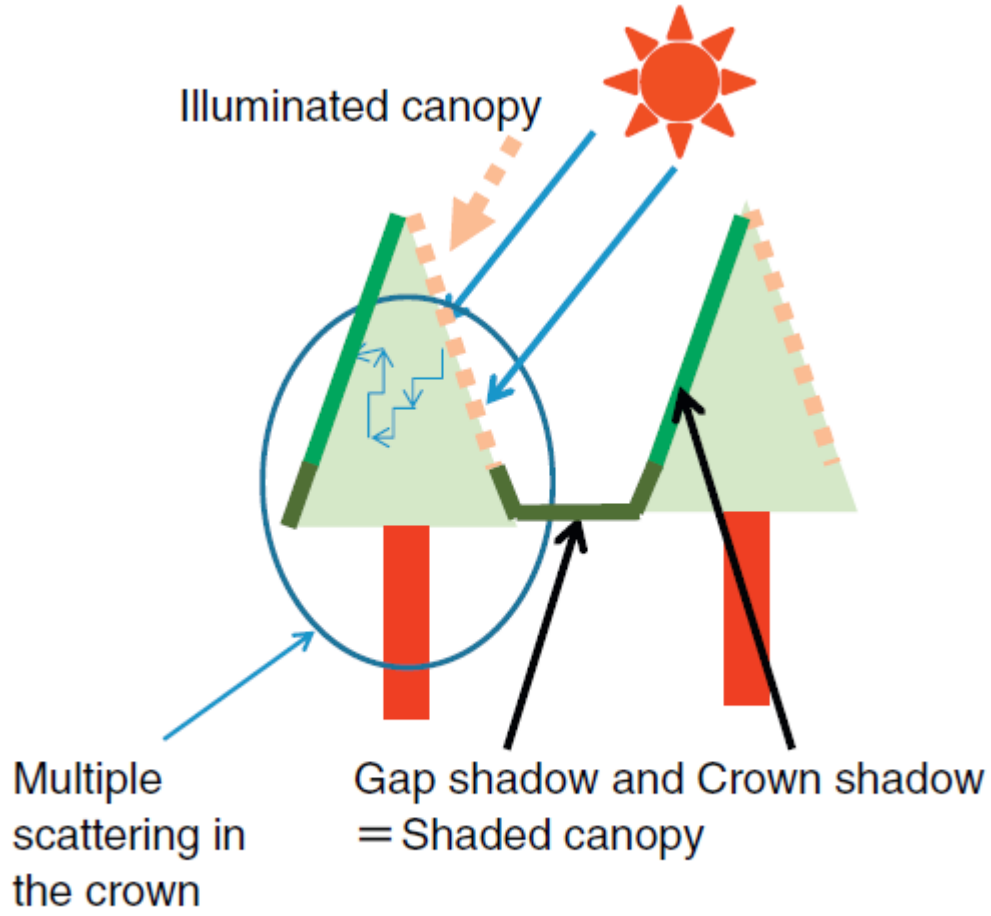

Fig. 13. Schematic illustration of crown shadow and gap shadow.

What a beautiful paper! “Why FLD is not working at coniferous forest site?” Is almost solved. I should make the SZA map in our TNF site and collect data continuously. The NIR band reflectance is like “s” curve. I think this is effect of SZA. First when the SZA is opposite from our sensor, then the signal is small, however, if the sun locates our side then, it should be blight because of scattering effect.

1st Feb

Rautiainen, M., Lukeš, P., Homolová, L., Hovi, A., Pisek, J., & Mõttus, M. (2018). Spectral Properties of Coniferous Forests: A Review of In Situ and Laboratory Measurements. *Remote Sensing*, *10*(2), 207.

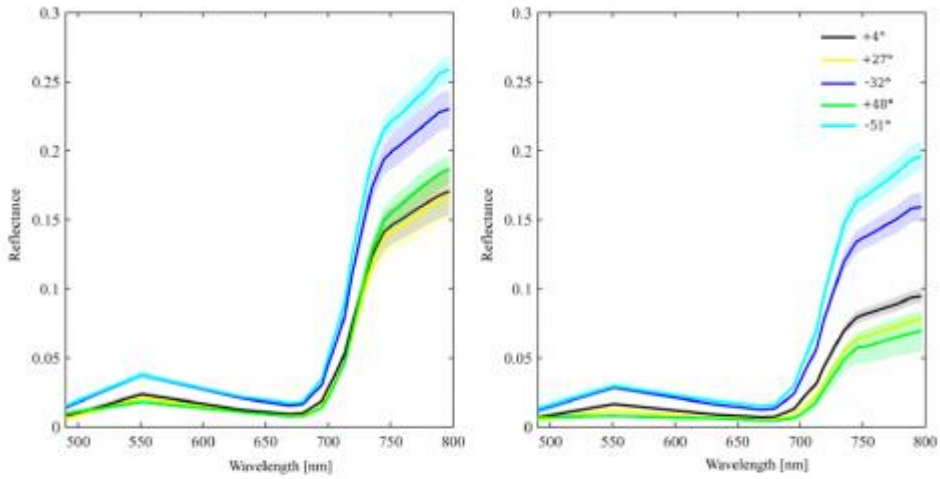

Figure 8. Top-of-canopy hemispherical-directional reflectance factors (HDRF) of immature (left) and mature (right) Norway spruce forest stands at Bílý Kříž site sampled in five angular observation geometries: near-nadir +4° (black), +27° (yellow), −32° (blue), +48° (green), and −51° (cyan) from nadir. Data were acquired by the CHRIS sensor onboard the tiltable PROBA satellite on 21 September 2007. Sun zenith angle during the data acquisition was 50° and azimuth 163°.

I think this is one of key paper about reflectance in coniferous site. When I tried to get peak signal in apparent reflectance within 761 nm, the peak signal is quite differenced over the solar zenith angle. I think this effect comes from coniferous characteristic such as scattering and trapping effect. I should cite this paper to get sif using FLD method.

4th Jan

Brusa, A., & Bunker, D. E. (2014). Increasing the precision of canopy closure estimates from hemispherical photography: Blue channel analysis and under-exposure. *Agricultural and Forest Meteorology*, *195*, 102-107.

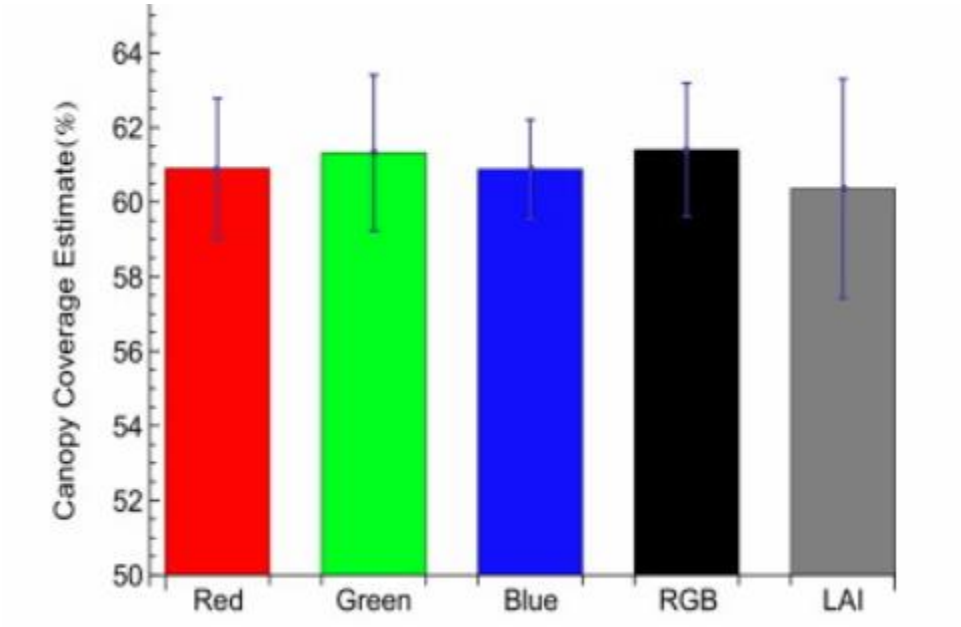

This paper showed why blue channel suitable for estimation of LAI. They tested improvements to hemispherical photography estimates of canopy closure. Blue channel analysis significantly decreased the variance of canopy closure estimates. Overexposed images had higher variance than auto- or underexposed images. Hemispherical photography performed similarly to Li-Cor LAI2200. Hemispherical photography is a cost-effective alternative for quantifying canopies.

3rd Jan

Lang, A. R. G., & Yueqin, X. (1986). Estimation of leaf area index from transmission of direct sunlight in discontinuous canopies. *Agricultural and forest Meteorology*, *37*(3), 229-243

I think this paper showed the clumping effect firstly. they have shown previously that the leaf area index of uniform crops can be determined by using the sun's beam as a probe. they show theoretically and empirically that the leaf area index of vegetation with large gaps can be measured by suitably averaging the local gap frequency, as detected by the transmission of the direct beam of the sun. They recommended that procedure is to average the transmission linearly over a horizontal path ten times the characteristic width of a leaf and take the logarithm of this mean. The average of logarithms for many such paths is shown to be linearly related to the leaf area index. My questions is what is the physical meaning of different location of averaged.

2nd Jan

Fang, H., Li, W., Wei, S., & Jiang, C. (2014). Seasonal variation of leaf area index (LAI) over paddy rice fields in NE China: Intercomparison of destructive sampling, LAI-2200, digital hemispherical photography (DHP), and AccuPAR methods. *Agricultural and forest meteorology*, *198*, 126-141.

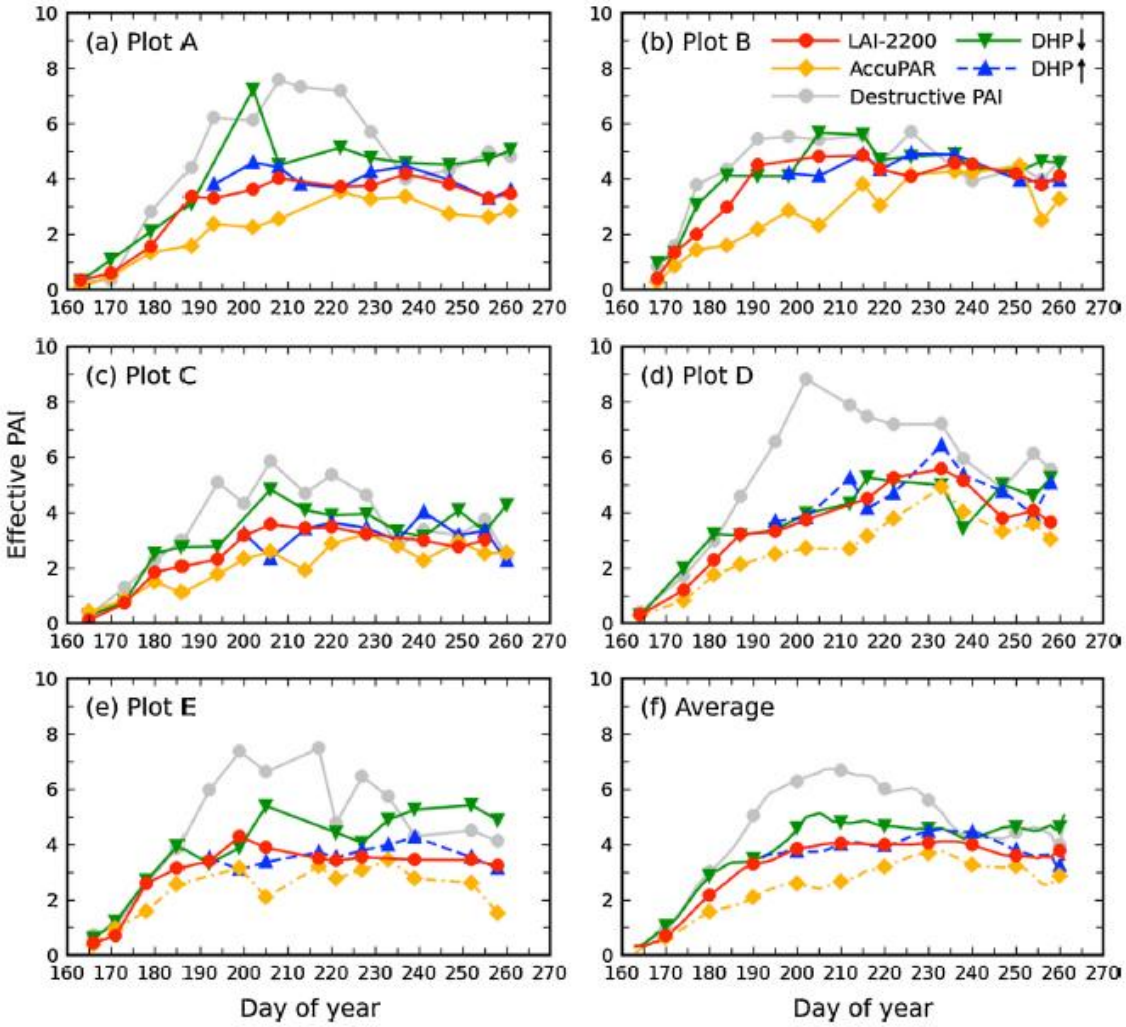

Wow. This paper really well organized the difference between DHP, LAI-2200, destructive sampling, and PAR to estimate LAI. Both LAI-2200 and DHP generate consistent effective PAI (PAIeff) estimates during the season (R2= 0.76, RMSE = 0.97). During the peak growing period, the high PAIeff(>3.5) and the very low gap fractions indicate that the multiple-scattering effect may have been suppressed to some extent with the new LAI-2200 configuration. My question is why did they suspect that effect of scattering affects the PAIeff? Why did they think LAI-2200 value is underestimated because LAI-2200 'see' stem and yellow, but, the photons are captured by leaves?

1st Jan

Wilson, J. W. (1960). Inclined point quadrats. *New Phytologist*, *59*(1), 1-7.

I think this paper is one of the key paper about K and G-function. the K(theta)is the extinction coefficient and G is the leaf projection function. It is hard to understand fully, but, I think this paper started focusing on the leaf angle and contribution. My question is why 57.5 degrees show conversion point?

Paper of the week 2018!!